A NEW METHOD FOR THE IN-SITU DIFFUSE REFLECTANCE FTIR ANALYSIS OF COALS

Dongtao Li, Wen Li, Haokan Chen and Baoqing Li

State Key Laboratory of Coal Conversion,
Institute of Coal Chemistry, Chinese Academy of Sciences,
030001, Taiyuan, P.R.China

Introduction

Since the first application of infrared spectroscopy in coal science made by Cannon et al.[1], it has been being used as the main characteristic method for coal. However, when the conventional transparent IR spectroscopy was used, KBr must be used to dilute the coal samples, which can result in many problems such as the adsorbing of moisture and catalyzing the pyrolysis of coal etc. Hence Fuller et al.[2] proposed to use the diffuse reflectance infra red spectroscopy (DRIFT) for the analysis of coal, and the disturbance from KBr was eliminated consequently. Moreover, it was proved to be possible to use neat coal samples for DRIFT, and since then this method has been used more and more widely in coal science. Moreover, because of the use of isolated reactor chamber this technique is very likely to be used for the in-situ analysis of coal. However, because of condensation of the volatiles produced by coals during pyrolysis, its application has been limited. In this paper, a new method that mainly deals with this problem is proposed, and it implied that this method could also be used for other samples that can produce volatiles when heated.

Experimental

Samples. The dimineralized (with HF/HCl) Huolinhe lignite was used. Sample of –100 mesh was further ground under argon for 30 min in a glove box with an agate mortar. Both proximate and ultimate analysis of the parent Huolinhe lignite (abbreviated as HLH) are given in **Table 1**.

Table 1 Analysis of samples

Sample	Proximate analysis (%)			Ultimate analysis (%, daf)				
	V (daf)	M (ad.)	A (ad.)	C	H	N	S	O (diff.)
HLH	48.42	17.38	25.56	73. 11	4. 70	1. 22	0.44	20.53

Apparatus and procedure. The diffuse reflectance spectra were measured on EQUINOX 55 FTIR spectrometer (BRUKER) with the 0030-102 high temperature/high pressure accessory of Thermo Spectra-Tech using ZnSe windows. The detector was liquid nitrogen cooled MCT (mercury cadmium telluride). A mirror that is believed not to absorb water was used as the background[3]. The DRIFT spectra were collected with the co-additions of 100 scans and resolution of 8 cm^{-1}. The resultant spectra were converted to Kubelka-Munk function.

Because of the condensation of volatiles produced from heated coal samples, a piece of porcelain was used. About 0.2~0.3mg coal samples was placed onto it and was pressed with a spatula, then the porcelain was placed into the center of the original reactor (**Figure 1**) and the dome was fixed. Before IR measurement, about 260ml/min argon was introduced for about 90 minutes for the stabilization of moisture adsorbed by sample. After that, the flow rate of argon was adjusted to 400 ml/min and the spectra of sample were collected from room temperature (26 ^{o}C) to 620 ^{o}C at every 30^{o}C when the sample was heated at a rate of 6 ^{o}C/min. The heating was manually controlled and the plot of temperature versus time is given in **Figure 2**. The accuracy of the temperature controlling is about ±1^{o}C, and the coefficient of fit linear result (Temperature [^{o}C]= 5.99835 ^{o}C/min)*Time[min.]+26.14465[^{o}C]) in **Figure 2** is >99.99%, hence this manually temperature-controlled heating is as good as automatically temperature-programmed-heating when the sample is heated slowly.

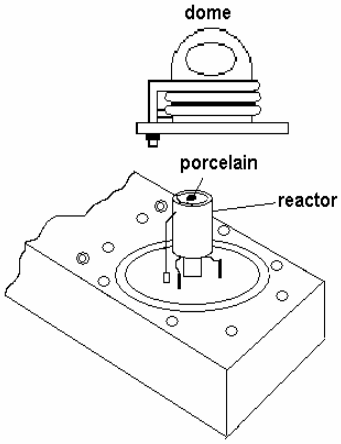

Figure 1 The schematic of the high temperature/high pressure reactor of Spectra-Tech[4].

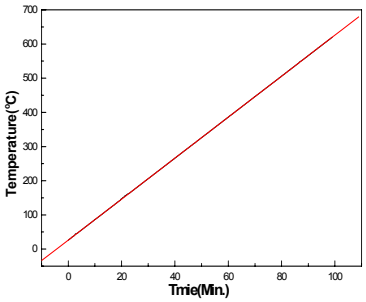

Figure 2 The manually temperature-controlled curve at a heating rate of 6^{o}C/min

Results and Discussion

The reliability of this method. For many researchers, the in-situ DRIFT analysis of coals from room temperature to high temperature is limited by the condensation of volatile produced by coal heated, and we also encountered this difficulty when we applied the commercial DRIFT accessory for our experiments. With the original commercial accessory, about 20 mg coal is needed, and even the argon was introduced at the rate of about 600ml/min, the condensation of volatile produced by coal could not be eliminated.

Fraser[5] and Iwanski[6] had proved that, for the DRIFT analysis, only the sample on the top 10 microns can contribute to the diffuse reflectance spectra of coal. When the reactor of the commercial accessory (with a depth of 2 mm and a diameter of 6 mm) were used, the amount of sample loaded into the reactor is too large, which is not necessarily needed for IR measurement. Volatile will condense on the windows and disturb the spectra of the solids consequently. Therefore, reducing and/or removing the amount of volatiles produced is probably the key to solve this problem.

In order to achieve this, two measures were taken. One is to reduce the amount of samples used so that the volatile matter produced is ignored. Obviously, it is impossible to reduce the amount

of sample loaded into the original reactor shown in **Figure 1**, because on the one hand it is required to press the samples in it so that the sample surface is smooth, which means that the reactor must be cramed; and on the other hand, the tip of thermocouple is just in the middle of the reactor, and it is not convenient to press the sample with a smaller spatula when only a thin layer of sample is loaded (in fact, this operation is not permitted, because the infrared light will be shut out by the wall of the reactor). To solve this difficulty, a piece of porcelain with a height of 2 mm (which is just the depth of the original reactor) and a diameter of 3 mm (which is the diameter of the section area of the infrared light) was used. About 0.2~0.3mg coal was placed on the top of it and pressed with a spatula. Finally the porcelain was placed into the center of the reactor provided by Spectra-Tech company (**Figure 1**). The subsequent experimental procedures are the same as those of using the original reactor. Another measure taken by us was increasing the flow rate of carrier gas so that the small amount of volatiles produced is purged out as soon as possible, and 400ml/min was set as the common flow rate used after optimization.

As for the amount of sample used, through calculating, it was proved that 0.2~0.3 mg coal is enough for the requirement on the height of sample in DRIFT analysis. In fact, only a layer of coal was needed if the diameter of coal particle were supposed to be 10 microns. So it is clearly that the amount of sample used is enough, while the amount of volatiles produced can been greatly reduced.

The spectrum of demineralized HLH (abbr. as HHD) measured at 620 ^{o}C with the original reactor, named A, and that with the porcelain, named C, are both shown in Figure 3. Unexpected absorbance was observed in spectrum A, particularly at the wavenumber of 2930cm^{-1} and 3560cm^{-1}, which is believed to be due to the tar and water condensed in ZnSe window respectively. We try to modify the spectrum A with abstraction of the effect of tar and water, the resultant spectrum named B showed that only the effect of tar could be partly eliminated, but the water disturbance still existed due to its strong absorption by tar. This suggested that only using the porcelain as the reactor, the true in-situ spectrum of the coal at high temperature could be obtained.

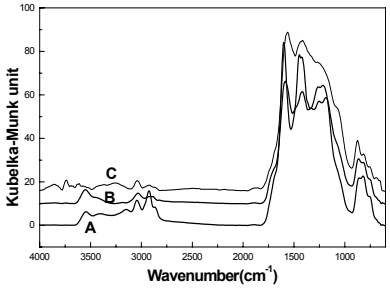

Figure 3 The spectra of HHD (A, measured with original reactor;
B, the spectrum after the subtraction of the contribution of tars condensed on windows; C, the spectrum measured with porcelain reactor.)

The spectra shown in **Figure 4** are measured directly by the spectrometer during the in-situ analysis of the same coal without any modifications, and the quality of them was found very good. When the variation trend of the spectra is compared with that in a reference [(7)], it was found almost the same as that proved by other researchers. Therefore, we think the method can be used for the in-situ analysis of coal with high reliability.

The keys of using this method. We have used this method successfully for the in-situ analysis of coal macerals and the kinetics of the decomposition of hydrogen bonds in coal. However, to get proper and reliable spectra, some cares should be taken. First, to press the coal sample placed on the top of porcelain, the surface of the sample pressed cannot reflect light when it is seen under light. Second, the porcelain should be placed just in the center of the reactor. Third, the flow rate of carrier gas should be as large as 400ml/min so that the small amount of volatiles produced was purged out as quickly as possible.

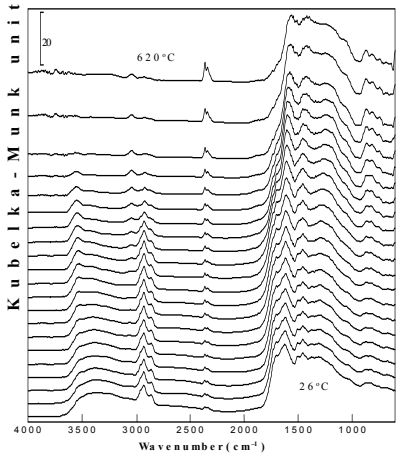

Figure 4 The in-situ DRIFT spectra of HHD from 26^{o}C to 620 ^{o}C measured at every 30^{o}C

Conclusions

Using a small porcelain (with a height of 2mm and a diameter of 3mm) to support coal, combined with increasing the flow rate of carrier gas, it is possible to get high quality spectra for in-situ DRIFT analysis of coal samples. With this method, the samples can be analyzed at as high as 620 ^{o}C or higher. We suggest this method is also useful for the in-situ analysis of other samples producing volatiles when heated.

Acknowledgement

This work was supported by the Natural Science Foundation of China, under contract No. 29906012. The authors gratefully acknowledge many valuable discussions with Prof. Dong Q in our institute.

References

(1) Cannon, C. G.; Sutherland G. B. M. *Transaction of Faraday Society*, **1945**, *41*, 279~288.
(2) Fuller M. P.; Griffiths, P. R. *Analytical Chemistry*, **1978**, 50(13), 1906~1910.
(3) Miura, K.; Mae, K.; Li W. et al.. Energy & Fuels, 2001,15(3), 599~610.
(4) *High temperature/High Pressure chamber (P/N 0030-102) User's Manual(Version 2.1)*, Spectra-Tech(USA), p. 3.
(5) Iwanski P. *Energy &Fuel*s, **1990**, 4, 589.
(6) Fraser, D. J. J.; Groffiths, P. R. *Applied Spectroscopy*, **1990**, 44 (2), 193.
(7) Solomon, P. R. Relation between coal structure and thermal decomposition products. In *Coal Structure: Advances in Chemistry Series, Vol. 192* (Edited by Gorbaty, M. L. and Ouchim, K.), American Chemical Society: Washington D. C., 1981, 95~112.

POTENTIAL OF STABLE NITROGEN ISOTOPE RATIO MEASUREMENTS TO RESOLVE FUEL AND THERMAL NO_x IN COAL COMBUSTION

Colin E. Snape[1], Chenggong Sun[1], Anthony E Fallick[2], Robin Irons[3], and John Haskell[3]

[1]Nottingham Fuel &Energy Centre, School of Chemical, Environmental & Mining Engineering, University of Nottingham, University Park, Nottingham NG7 2RD, UK

[2]Scottish Universities Research & Reactor Centre (SURRC), Rankine Avenue, East Kilbride Glasgow, G75 0QF, UK

[3]Power Technology Centre, Powergen, Ratcliffe-on-Soar, Nottingham, NG11 0EE, UK

Introduction

Atmospheric stable nitrogen isotope ($\delta^{15}N$) measurements on NO_2 suggest that significant differences may exist between NO_x derived from coal and that from transport fuel sources [(1)], which predominantely is formed from air nitrogen via thermal and prompt meachanistic pathways. However, thus far, no nitrogen isotopic data have been reported directly for NO from coal combustion due to the problems of first adsorbing the NO and then determining the $\delta^{15}N$ of the NO which, in terms of minimizing sample size and maximizing throughput is best achieved using an elemental analyzer linked to an isotope ratio mass spectrometer (EA-IRMS). If fuel and thermal NO_x can be quantified, this will be an important development to help guarantee combustor performance and aid combustion modeling.

To address the issue of whether a significant isotopic difference exist between prompt/thermal and fuel NO_x in PF combustion of coal, we describe the development of a nitrogen-free active carbon for adsorbing NO. The preparation is based on previous work that has indicated promising substrates that can adsorb sufficiently large quantities of NO_x to meet the requirements for subsequent isotope analysis include zirconia supported manganese (MnO_y-ZrO_2) [(2)], and active carbon supported iron oxide (Fe/AC)[(3,4)] promoted by other metals including cerium. The nitrogen free Fe/AC sorbent prepared here is used to determine, for the first time, the $\delta^{15}N$ values for thermal and actual NO from PF coal combustion. In addition, we report the stable isotope values for a number of combustion chars to help explain the isotopic fractionation that occurs during PF combustion.

Experimental

Preparation of the N-free sorbent Granulated white sugar purchased from a local supermarket was used. About 200 g of this sugar was first dehydrated in ~ 250 ml concentrated sulfuric acid to produce a char-like porous solid. This solid material was then washed using excess distilled water and dried in an air-blown oven at 60°C. The dried solid material was then carbonised at 650°C for about 3 hours in a fixed-bed reactor to yield the sugar-based char, which was subsequently activated at 1000 °C in a flow of CO_2 (~90 min.) in order to obtain the final sugar-based activated carbon product. For 100 g of sugar, about 15~20 g of activated carbon can be obtained from this procedure.

In order to prevent any nitrogen incorporation during the sorbent preparation, the use of nitrogen-bearing chemicals was avoided. The sugar-based AC material was first treated in 0.2 N $KMnO_4$/0.5 N KOH solution for about 5 hrs and, subsequently, the same volume of 0.5M N $Fe_2(SO_4)_3$ solution was poured into the mixture. The pH of the new mixture was controlled at 12 and the mixture was then stirred for 5 hrs before it was filtrated, washed with distilled water and dried at 120°C. The dried raw sorbent material was then calcined at 500°C for 10 hrs to obtain the final Fe-Mn/AC sorbent.

Laboratory measurements indicated that, with a typical flue gas composition, the breakthrough for NO corresponds to a nitrogen uptake of over 0.5 % w/w.

NO_x sampling and analysis A thermal/prompt and an actual PF NO_x sample have been collected in duplicate from a 1 MW test facility at Powergen. The sampling time available enabled nitrogen uptakes as NO of approximately 0.1-0.2% to be achieved without any NO breaking through the adsorbent bed (*ca*. 2 g). The thermal NO sample was collected when the PF facility was starting up with a fuel oil containing litttle nitrogen (0.1% cf. 1-2% for coals). The NO samples and the blank sorbent have been analysed using a Europa EA-IRMS instrument with 4 determinations being carried out for each of the NO_x samples. System blanks were measured before and after each set of replicates for the five samples. Seven determinations were also carried out on the sorbent blank. In addition to the NO_x samples, a number of coals and a series of char samples has also been analysed using the same instrument.

Results and Discussion

Coals The nitrogen stable isotope values for a number of coals using the standard permil notation references to atmospheric nitrogen are listed in Table 1. The $\delta^{15}N$ values all occur over the relatively narrow range of + 1-4 ‰ with the range being even smaller for the UK coals with all the values being close to +2 ‰.

Table 1 A summary of stable nitrogen isotope ratios for a selection of coals.

Coal	*$\delta^{15}N$, ‰*
Blair Athol, Australia	1.6
Ensham, Australia	1.5
Gedehoop, South Africa	1.4
Irui, Brazil (high ash, high vol.)	3.8
Polish coal	2.6
Prodeco, Colombia (high vol.)	0.6
N. Dakota lignite, USA	2.2
Marrowbone, (USA, high vol.)	2.5
Walter, USA (low vol., Alabama)	1.4
Daw Mill, UK	2.6
Harworth, UK	1.8
Gascoigne Wood, UK	2.6

Table 2. Interferences (m/z of 28) in EA-IRMS for determination of nitrogen stable isotope ratios

	Total ion beam, A	% N (20 mg)
1. System background	2-3 x 10^{-10}	0.002
2. Sample		
(a) inherent N content (AC)	0.5-3 x 10^{-8}	0.05-0.2
(b) comb. catalyst, V_2O_5	1.5-3 x 10^{-9}	0.01-0.02

Thermal/prompt and actual PF NO_x samples Before discussing the $\delta^{15}N$ values for the NO samples, it is important to assess the interferences that can arise in the EA-IRMS. Table 2 lists the interferences in terms of current observed which is translated into a nitrogen content for a 20 mg samples size which was largely used throughout this study. The system background (empty sample capsule) corresponds to 10% of the count obtained with the combustion catalyst in the sample capsules. However, the ion

currents obtained with active carbons containing appreciable nitrogen contents are an order of magnitude greater still. This summary indicates the necessity to work with adsorbents containing extremely low nitrogen contents.

The results for the NO_x samples and the sorbent blank (no NO adsorbed) are presented in Table 3. The total beam intensity for these analyses did not vary systematically with sample weight but averaged 3.1 x 10^{-9} A; this compares to an average system blank of (1.9 x 10^{-10} A over the course of the entire experiment. For a 20 mg sample size, this corresponds to a nitrogen content of *ca*. 0.01%.

For the four replicates of the first thermal NO (1A) sample, the mean %N was (0.125 ± 0.006) and the mean $\delta^{15}N$ was -6.2 ± 1.3‰ (Table 3). The average total beam was 1.96 x 10^{-8}A meaning that the sorbent blank represents 16% of the sample total beam. No correction was made here. For the four replicates of the second thermal NO sample (1B), the mean %N was 0.09 ± 0.00 and the total beam of 1.44 x 10^{-8}A meant that the sorbent blank represents 21.5% with a mean $\delta^{15}N$ = -6.1 ± 0.5 ‰. The two mean values for thermal samples 1A and 1B are indistinguishable, supporting the decision not to correct for the blank. For the 8 replicates of the thermal NO_x samples, the mean $\delta^{15}N$ was -6.2 ± 0.9 ‰.

Table 3 Thermal/prompt and actual PF NO_x samples collected with the nitrogen-free Fe/AC adsorbent

Sample/ Determin. no.	Weight mg	Total Beam A	% N	$\delta^{15}N$ ‰ air
1. sorbent blank	10.8	3.87 10^{-9}	0.02	37.1
2. sorbent blank	16.0	3.13 10^{-9}	0.01	-0.7
3. sorbent blank	20.9	2.73 10^{-9}	0.01	-4.1
4. sorbent blank	24.9	3.16 10^{-9}	0.01	-12.0
5. sorbent blank	20.4	3.18 10^{-9}	0.01	13.2
6. sorbent blank	15.7	2.98 10^{-9}	0.01	28.0
7. sorbent blank	10.4	2.68 10^{-9}	0.02	7.1
1. Thermal 1A	20.7	1.95 10^{-8}	0.12	-4.7
2. Thermal 1A	19.5	1.94 10^{-8}	0.13	-5.6
3. Thermal 1A	19.5	1.93 10^{-8}	0.13	-7.5
4. Thermal 1A	20.9	2.02 10^{-8}	0.12	-7.0
1. Thermal 1B	19.6	1.42 10^{-8}	0.09	-6.7
2. Thermal 1B	20.1	1.49 10^{-8}	0.09	-5.6
3. Thermal 1B	21.1	1.43 10^{-8}	0.09	-6.1
4. Thermal 1B	19.3	1.41 10^{-8}	0.09	-6.1
1. PF 2A	19.1	3.52 10^{-8}	0.23	15.1
2. PF 2A	21.2	3.90 10^{-8}	0.23	14.5
3. PF 2A	20.8	3.89 10^{-8}	0.24	13.8
4. PF 2A	20.5	3.82 10^{-8}	0.23	14.4
1. PF 2B	20.8	3.41 10^{-8}	0.21	18.1
2. PF 2B	19.9	3.06 10^{-8}	0.19	14.4
3. PF 2B	20.0	3.06 10^{-8}	0.19	14.8
4. PF 2B	20.5	3.04 10^{-8}	0.19	13.2

For four replicates of the actual PF sample (1B), the mean %N was 0.23 (± 0.00) and mean $\delta^{15}N$ was 14.5 ± 0.5 ‰ (Table 3). The mean total beam intensity was 3.78 ± 0.18 10^{-8} A so the sorbent blank represents 8 %. For the second sample, the mean %N was 0.19 ± 0.01 with $\delta^{15}N$ of 15.1 ± 2.1‰. The mean total beam intensity was 3.14 x 10^{-8} A so the sorbent blank represents 10%. Again, no correction has been made here and again the means for the PF samples 2A and 2B are isotopically indistinguishable, with the overall average from the eight measurements being 14.8 ± 1.5 ‰. These measurements indicate that differences of up to *ca*. 20 ‰ can exist between thermal and PF fuel (char) NO_x isotopic values.

Table 4 Nitrogen stable isotope ratios for combustion chars prepared in a drop tube reactor from 3 coals

Sample/drop tube resience time		% N w/w	$\delta^{15}N$ ‰ air
1. Oreganal	200 ms a	1.92	4.2
(Colombia)	200 ms a	2.28	3.9
	200 ms b	2.15	3.3
	200 ms b	1.82	4.3
Mean $\delta^{15}N$ ‰			*3.9*
	400 ms a	1.24	4.8
	400 ms a	1.13	4.2
	400 ms b	1.37	5.7
	400 ms b	1.83	5.4
Mean $\delta^{15}N$ ‰			*5.0*
	600 ms a	0.37	5.9
	600 ms a	0.29	6.4
	600 ms a	0.54	5.5
	600 ms b	0.82	5.3
	600 ms b	0.93	5.5
Mean $\delta^{15}N$ ‰			*5.7*
2. Kaltima Pr.	200 ms a	2.02	3.9
	200 ms a	2.28	2.6
	200 ms b	1.72	3.9
	200 ms b	2.24	2.1
Mean $\delta^{15}N$ ‰			*3.1*
	400 ms a	2.19	4.1
	400 ms b	2.28	4.6
	400 ms b	1.74	3.3
Mean $\delta^{15}N$ ‰			*4.0*
	600 ms a	0.80	4.2
	600 ms a	0.63	2.4
	600 ms b	1.40	4.1
	600 ms b	1.30	2.8
Mean $\delta^{15}N$ ‰			*3.3*
3. Pocahontas	200 ms a	1.38	5.3
	200 ms a	1.40	6.0
	200 ms b	1.28	6.1
	200 ms b	0.92	5.7
Mean $\delta^{15}N$ ‰			*5.8*
	400 ms a	0.65	6.5
	400 ms a	0.76	6.5
	400 ms b	1.17	6.9
	400 ms b	1.38	6.4
Mean $\delta^{15}N$ ‰			*6.6*
	600 ms a	0.76	6.3
	600 ms a	0.85	6.4
	600 ms b	0.73	5.9
	600 ms b	0.95	7.2
Mean $\delta^{15}N$ ‰			*6.5*

Char analysis Table 4 lists the nitrogen stable isotope ratios for a series of partially combusted chars prepared at different residence times (200, 400 and 600 ms) in a drop-tube reactor from

three different coals. Pyrolysis chars from each coal were prepared in the drop tube reactor and these were then fed back into the reactor using an atmosphere containing 5 % oxygen. Two separate char samples were analysed for each residence time. Of the 3 coals investigated, the Indonesian coal (Kaltima Prima) is the most reactive and Pocahontas (USA) the least.

In all cases, the nitrogen stable isotope ratios of the chars are heavier than than those of coals and range from 3 to 7 ‰. However, Table 4 indicates that the isotopic fractionation is roughly in the order Pocahontas > Oreganal > Kaltima Prima, which is the opposite trend to that in reactivity. For the two least reactive coals, the extent of isotopic fractionation increases with burnout (cf. 600 with 400 and 200 ms chars in Table 3 for Pocahontas and Oreganal). Table 5 lists the stable nitrogen isotopic ratios for a Spanish coal, a pyrolysis char and four combustion chars obtained at high levels of burnout. The data for the Spanish coal reveal that the nitrogen stable isotope ratios of combustion chars obtained at high levels of burnout do not change markedly (Table 5).

In conclusion, it would appear that much of the isotopic fractionation that occurs between coal nitrogen and fuel NO occurs in the formation of char, although further fractionation can be inferred to occur during char combustion. In contrast, a lesser degree of isotopic fractionation is associated with the formation of thermal NO (*ca*. –6 ‰), atmospheric nitrogen having a value of 0 ‰.

Table 5 Nitrogen stable isotope ratios of a Spanish coal, a pyrolysis char and three combustion chars prepared in a drop tube reactor

Sample	% N	$\delta^{15}N$	
1. Coal	2.27	2.5	Mean 2.5
	2.12	2.5	
2. Pyrolysis char	1.51	4.7	Mean 4.5
	2.28	4.3	
3. Combustion char,.	N.D.	5.7	Mean 6.0
86 % burnout	1.98	6.3	
4. Combustion char,	1.54	5.7	Mean 5.6
93 % burnout.	1.44	5.4	
5. Combustion char,.	4.9	5.1	Mean 5.3
95 % burnout	5.6	5.4	
6. Combustion char,	5.1	5.2	Mean 5.5
97 % burnout.	6.0	5.7	

Conclusions

The fact that differences of up to *ca*. 20 ‰ can exist between thermal and PF fuel (char) NO_x isotopic values augurs well for the further development of the approach to help quantify the extent of thermal/prompt NOx formation in PF combustion. However, measurements on char have indicated that the extent of isotopic fraction that occurs between coal-N and NO_x from char is related to the reactivity of coals. We will report shortly the stable isotope ratios of NO_x samples collected under a variety of PF combustion conditions.

Acknowledgement. The authors thank the UK Department of Trade and Industry (DTI) for financial support (coal programme, contract no. 231). We thank Dr. Ana Arenillas (INCAR) and Dr. E. Lester (Univ. of Nottingham) for supplying the char samples and Mitsui Babcock (Dr S.C. Mitchell) for technical assistance.

References

(1) Heaton,. T. H. E.: *Atmospheric Environm*., **1987**, *21*, 843.
(2) Eguchi, K. and Hayashi T. *Catalyst Today,* **1998**, *45*, 109.
(3) Kaneko, K. and Inoyue, K. *Carbon*, **1986**, *24*, 772.
(4) Kaneko, K., Ozeki, S. and Inouyue: K., *Atmospheric Environm*, **1987**, *21*, 2053.

PROBING COAL HETEROGENITY ON THE NANOSCALE BY NMR

Robert E. Botto and David L. VanderHart^*

*Chemistry Division, Argonne National Laboratory, 9700 S. Cass Ave., Argonne, IL 60439 and Polymer Division, National Institute for Standards and Technology, Gaithersburg, MD

Introduction

Exploring chemical and materials' properties on the nanometer scale presents significant challenges. Characterization methods such as neutron and x-ray scattering, diffuse-reflectance infrared spectroscopy and nuclear magnetic resonance (NMR) spectroscopy are being applied to probe variations in chemistry on the nanoscale. However, many challenges remain when studying extremely complex, heterogeneous substances. Several obstacles are not easily overcome, particularly when applying NMR techniques to structurally complex fossil resources.[1]

Work carried out during the past decade in our laboratory has focused on identifying the variation in chemistry of complex carbonaceous solids. One particular focal point of our work has been on a study of coals from the Argonne Premium Coal Sample Program. Coal has been described as being an "organic rock" comprised of different plant remains that have been geologically altered over time, and as such, are considered to be extremely heterogeneous in nature. We have tried to address the following question: "On what length scale does the chemical heterogeneity in coal end?"

Earlier experiments have provided some insight into this question. Magnetic resonance imaging (MRI), [2,3] and more recently, synchrotron-based scanning transmission x-ray microscopy (STXM)[4,5] have provided detailed, two- and three-dimensional pictographs showing the chemical variation of the organic phases of coal. As an example, a carbon STXM micrograph highlighting microspores (magenta colored regions) within a thin section of Pittsburgh No. 8 coal (APCS 4) is shown in Figure 1 below. While the images obtained show a definitive, sharp separation in chemistry along maceral (metamorphosed plant organic matter) boundaries, the maximum image resolution that could be achieved was 50-100 nm at best, which lies on the upper limit of the nanoscale.

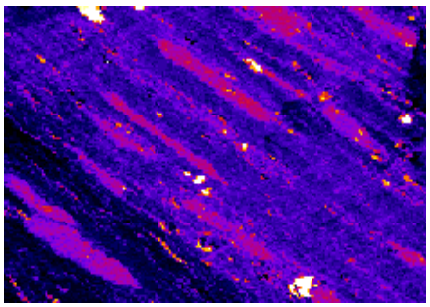

Figure 1. STXM micrograph of a thin section of Pittsburgh No. 8 Bituminous coal (APCS 4) recorded at an absorption energy of 285.5 eV (carbon π^*-aromatic absorption); clear white features in the image are holes.

In principle, spin-diffusion NMR techniques are capable of probing chemical heterogeneity on a scale of a few nanometers. These methods have been applied successfully to the study of phase-separated polymer blends whose components have sufficient chemical distinction.[6-8] The concept behind the experiment is to establish a magnetization gradient, or non-equilibrium magnetization condition, between the chemically different protons that reside in different domains, and then to allow the magnetization to equilibrate, or to 'diffuse' through domains. From the time dependence of the diffusion process, one can estimate the size of the domains. The challenge has been to apply the method to a substance as complex as coal, whose CRAMPS spectra seldom display more than two broad resonance bands associated with aromatic and aliphatic protons.

In this paper, we demonstrate the utility of proton spin diffusion methods for determining the size of submicroscopic resinite domains in Utah Blind Canyon coal (APCS 6) on a length scale down to a few nanometers.

Experimental Section.

Sample Preparation. A solid block of Utah Blind Canyon coal (APCS 6), which is a predominantly bimaceral coal comprised of resinite and vitrinite, was machined into a cylinder to match the exact internal dimensions of Bruker 7-mm diameter MAS rotors. The sample remained intact throughout the entire study.

Solid-State NMR Spectroscopy and Spin Diffusion. Solid-state proton NMR experiments were recorded on a Bruker Instruments spectrometer, model CXP-200, in the pulsed Fourier-transform mode. Combined rotation and multipulse spectroscopy (CRAMPS)[9] was used both to narrow the proton resonance lines and to establish a chemical-shift based polarization gradient for implementation of the proton spin diffusion experiment designed to probe domain size.[10] The polarization gradient was established by varying the duty cycle between pulses in the CRAMPS experiment to give a negative aromatic proton polarization and a positive aliphatic proton polarization. Proton signal was recorded after a variable delay period to allow for spin diffusion. Proton spin-lattice relaxation times were measured by using the standard inversion recovery method followed by CRAMPS readout of the proton magnetization.

Results and Discussion

Proton NMR experiments, both inversion-recovery and spin-diffusion types, employing CRAMPS (combined rotation and multiple pulse spectroscopy) methods were performed on a sample of Utah Blind Canyon coal (Argonne Premium Coal Sample No. 6), which is largely a bimaceral coal composed of vitrinite with about 7% resinite. Pure maceral fractions were obtained by physical separation methods in order to measure proton NMR spectra and proton relaxation times on the pure macerals, information that is needed to perform the analyses. Inversion-recovery data for measuring the longitudinal proton relaxation time, T_{1H}, is shown in Figure 2. The T_{1H} relaxation time decays of the resinite and vitrinite polarizations are distinct and the resinite line shape is extracted from this data based on two characteristics, namely, a) that line width for resinite is significantly narrower than for vitrinite and b) that T_{1H}'s of the vitrinite and resinite are distinct and quantifiable. Thus, knowing the general aliphatic line shape from the CRAMPS spectrum of each maceral, one can separate the resinite spectrum appropriate to this mixed sample from the inversion recovery data. The resinite spectrum is isolated when the broader aliphatic vitrinite component passes through the null condition. Note in Figure 2 that the resinite polarization does not decay exponentially for all time. Nevertheless, the fact that the T_{1H} decays are separable and, in particular, that the resinite component, representing about 20% of the total protons, has an upward rather than a downward deviation from exponential behavior, implies that most of the resinite domains exceed 100 nm in size.

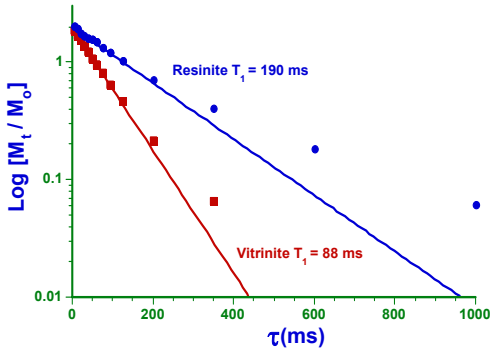

Figure 2. Proton magnetization decay curves and estimated spin-lattice relaxation times (T_1^H) for Utah Blind canyon coal (APCS 6).

We were also interested in the possibility that there might be some resinite domains, which were significantly smaller and within spin diffusion (SD) distances. The CRAMPS preparation chosen produces a modestly negative aromatic and a more strongly positive aliphatic proton polarization. An initial gradient of proton polarization is established between the two maceral phases, thereby allowing the use of the CRAMPS line shape to monitor any subsequent SD between those components. Changes in relative polarization levels of resinite and vitrinite domains with diffusion time are shown in Figure 3 with P_o representing the polarization at Boltzmann equilibrium. Only data for > 4 ms are included, because intra-phase equilibration dominates at earlier times. There is a reproducible, slightly accelerated rate of decay for the resinite polarization (see results in Figure 4), and a correspondingly, hardly perceptible rise in the vitrinite polarization in the 4 ms to 12 ms range. The deduction from Figure 4 in terms of mixing is that a maximum of 20% of the resinite protons are in domains small enough (< 6 nm) to undergo SD on the timescale of 12 ms or less. However, the majority of the protons of resinite are isolated from those of the vitrinite so that the resinite decay rate seen is indistinguishable from the resinite T_{1H} observed in the inversion-recovery experiment. From the similarity of slope for the SD and inversion recovery data for resinite, it is clear that most of the resinite is found in domains large enough (> 100 nm) so that SD on a time scale of 250 to 1000 ms has an insignificant effect on the rate of decay.

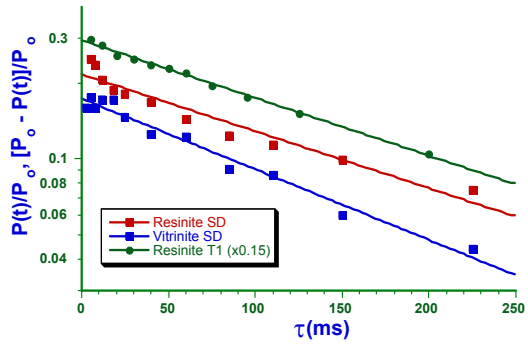

Figure 3. Proton magnetization decay curves for spin-lattice relaxation in resinite and spin diffusion in resinite and vitrinite.

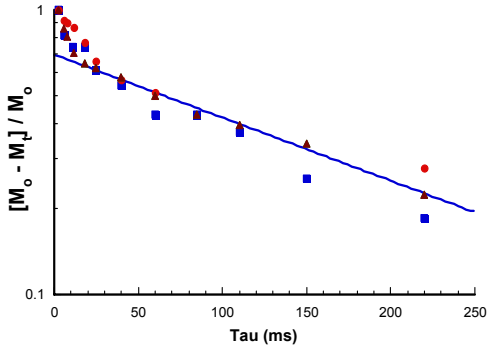

Figure 4. Summary of proton magnetization decay curves of spin diffusion for resinite domains in Utah coal.

Conclusions

The findings suggest that while most of the resinite inclusions found in the Utah coal are relatively large in size, consistent with the previous images obtained by STXM, there is a significant fraction of resinite material that is submicroscopic in size. These submicroscopic inclusions are about 6 nm or less, and represent about 20% of the resinite in the Utah coal. They have not been identified previously. Their existence can be explained by a geological process whereby small molecular weight resins produced in the plant epithelial cells were preserved throughout the woody micro-pores, and subsequent burial and diagenesis led to their ultimate polymerization to form small resinite inclusions intimate with the vitrinite matrix. These findings are entirely in accord with the known paleobotany and geochemistry of resins in coal bearing formations, and explain some of the unusual properties (reflectance, fluorescence, H/C ratio, and f_a) of the vitrinite in the Utah coal.

Acknowledgement. This work was performed under the auspices of the Office of Basic Energy Sciences, Division of Chemical Sciences, Biosciences and Geosciences, U. S. Department of Energy, under contract number W-31-109-ENG-38.

References

(1) Cheung, T. T. P.; Gerstein, B. C. *J. Appl. Phys.*, **1981**, *52* (9), 5517.
(2) Dieckman, S. L.; Gopalsami, N.; Botto, R. E. *Energy Fuels,* **1990**, *4* (4), 417.
(3) French, D. C.; Dieckman, S. L.; Botto, R. E. *Energy Fuels,* **1993**, *7*, 90.
(4) Botto, R. E.; Cody, G. D.; Kirz, J.; Ade, H.; Behal, S.; Disko, M. *Energy Fuels,* **1994**, *8*, 151.
(5) Cody, G. D.; Botto, R. E.; Kirz, J.; Ade, H.; Behal, S.; Disko, M.; Warick, S. *Energy Fuels,* **1995**, *9*, 525.
(6) Havens, J. R. ; VanderHart, D. L. *Macromolecules*, **1985**, *18* (9), 1663.
(7) Vanderhart, D. L.; McFadden, G. B. *Solid State Nucl. Magn. Reson.*, **1996**, *7*, 45.
(8) Neagu, C.; Puskas, J. E.; Singh, M. A.; Natansohn, A. *Macromolecules*, **2000**, *33*, 5976.
(9) Gerstein, B. C. *Philos. Trans. R. Soc. London*, **1981**, *A299*, 521.
(10) Campbell, G.C.; VanderHart, D. L. *J. Magn. Reson.,* **1992,** *96* (1), 69.

FOLLOWING COKE FORMATION BY CARBON-13 SOLID-STATE NMR

1. Menezes, Sonia M.C.
2. Sugaya, Marcos F.
3. Silva, Naira M.
4. Emmerich, Francisco G.
5. Girelli, Carlos M.A.
6. Rajakopal, Krisnaswamy

1,2. PETROBRAS/CENPES, Ilha do Fundão – Quadra 7, Cidade Universitária, 21949-900 – Rio de Janeiro, RJ, Brazil, sonia@cenpes.petrobras.com.br
3. PUC –Departamento de Química, Rio de Janeiro, RJ - Brazil
4,5. UFES, Lab. de Materiais Carbonosos, Vitória, ES - Brazil
6. UFRJ, Escola de Química, Rio de Janeiro,RJ - Brazil

Introduction

Coke is produced in petroleum refineries mostly by the delayed coking process. One of the difficulties in studying the chemical reactions involved in this process lies in the fact that the composition of petroleum distillation residues is largely unknown. The available analytical methods are very limited because of the large number of complex molecules involved. Only average properties can be obtained, making the attainable description of the system very poor. This contribution explores the coking process of a vacuum distillation residue using solid state nuclear magnetic ressonance (NMR) to characterize the thermal craking and condensation reactions taking place.

The reactions were followed mostly by cross polarization and magic angle spinning (CP/MAS) ^{13}C NMR. Non-quaternary supreesion (NQS) and a quantitative MAS experiments were also used. With those techniques it was possible to distinguish bridged aromatic carbons from protonated ones and also aliphatic carbons.

Experimental

SAMPLES. Vacuum destillation residue from the refining of a brazilian petroleum was processed on a laboratory furnace (Figure1) simulating the conditions in industrial delayed coking drums. The samples were treated at different temperatures varying from 440°C to 500°C. For each temperature the residence time at the furnace was varied from 0 to 4h.

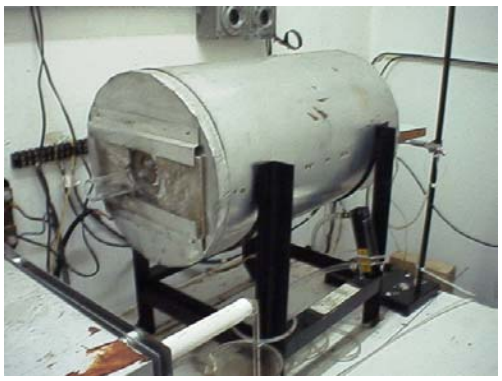

Figure 1. Laboratory furnace used for the coking studies

NMR. The experiments were conducted at room temperature using a Varian INOVA-300 (7.1T) NMR spectrometer operating at 75.4 MHz for ^{13}C. For the CP/MAS experiments a pulse width of 5.5 µs was applied with a delay time of 3s and 8000 transients were accumulated. A spectral width of 50 kHz and an acquisition time of 0.05s were used for data collection. The contact time was 4000 µs. The spectra were referenced to the hexamethylbenzene (methyl peak at 17.3 ppm from TMS). The pulse power was calibrated to achieve Hartmann-Hahn conditions. The samples were spun at 4.5KHz at MAS (54.7°) in a 7mm zirconia rotor. The NQS experiments used the same conditions of the CP/MAS and a decoupling window of 60µs. The MAS experiments were acquired using a 100s pulse delay and a 1000 transients. All spectra were processed using a 70Hz line broadening and a 0.004s gaussian function.
Spectra were integrated for the following resonance intervals: 100 to 165ppm (aromatic carbons) and 0 to 80ppm (aliphatic carbons). Corrections for sidebands contributions were considered for spectra calculations.

Results and Discussion

CP/MAS and NQS are faster but non-quantitative experiments. For one sample a variable contact time experiment was acquired in order to choose the contact time that mostly reproduces a quantitative MAS analysis. This condition was achieved at 4000µs. The CP/MAS and MAS experiments provided the total distribution of carbons present in a sample. The NQS experiment distinguishes quaternary carbons and also the methys when they are present.

Figure 1 shows typical ^{13}C MAS, CP/MAS and NQS spectra for one of the coke samples. The MAS and CP/MAS spectra, regions from 0 to 80 ppm and 100 to 165ppm are attributed to the aliphatic and to total aromatic (quaternary plus protonated) carbons, respectively. On the NQS spectra the signals from 100 to 165 ppm are due to quaternary carbons.

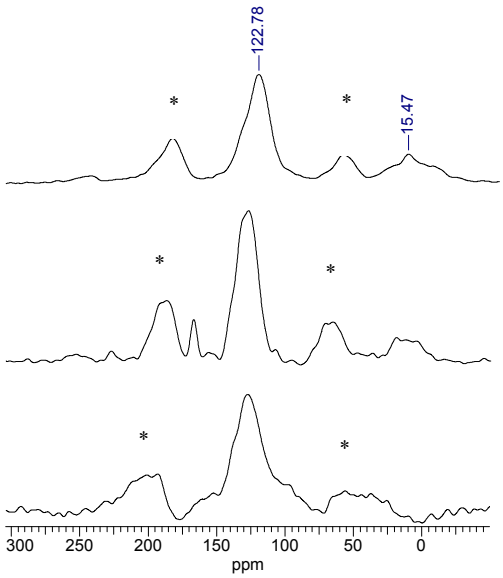

Figure 1. Coke sample treated at 440°C for 2 hours (TT 440-2H): ^{13}C MAS (top), CP/MAS with 4000µs contact time (midle) and NQS with a 60µs of decoupling window (bottom).
* spinning sidebands

In order to get the total distribution of carbons in the samples the quaternary aromatic carbons obtained by the NQS spectra were related to the total aromatic carbons from the CP/MAS spectra. The protonated carbons were obtained subtracting the total aromatic and

quaternary aromatic carbons. Aliphatic carbons were calculated from MAS spectra. Table 1 sumarizes the results.

Table 1. Carbon distribution of coke samples

SAMPLES	AROMATIC CARBONS (%)			ALIPHATIC (%) (0 - 80ppm)
	Total (100 - 165ppm)	Quaternary	Protonated	
Vacuum residuel	48,0	36,2	11,8	52,0
TT440 –0H	62,6	27,7	34,9	37,4
TT440 – 30min	79,7	39,5	40,2	20,3
TT440 –1H	85,0	35,0	50,0	15,0
TT440 –2H	85,5	41,8	43,7	14,5
TT440 –4H	86,0	66,4	19,6	14,0
TT460 –0H	70,7	26,5	44,2	29,3
TT460 – 30min	87,9	45,3	42,6	12,1
TT460 –1H	87,2	53,4	33,8	12,8
TT460 –2H	86,3	43,2	43,1	13,7
TT460 –4H	93,2	79,3	13,9	6,8
TT480 –0H	83,7	44,5	39,2	16,3
TT480 – 30min	88,6	51,3	37,3	11,4
TT480 –1H	87,9	42,7	45,2	12,1
TT480 –2H	88,4	47,4	41,0	11,6
TT480 –4H	93,9	54,0	39,9	6,1
TT500 –0H	80,9	23,6	57,3	19,1
TT500 – 30min	89,0	31,6	57,4	11,0
TT500 –1H	86,8	37,3	49,5	13,2
TT500 –2H	92,8	48,0	44,8	7,2
TT500 –4H	89,2	32,4	56,8	10,8

The results indicated well the increase of the percentage of total aromatic carbons as the temperature and residence time increase. It was also observed that quaternary aromatic carbons has raised with residence time for a given temperature. These were somehow expected although at 500°C the aromatic quaternary carbons surprinsingly presented lower values.

At industrial delayed coking units the temperature of the coking drums usually stays between 490°C (bottom) and 440°C (top). The data showed at Table 1 indicated that the thermal cracking and condensation reactions leading to the final composition (high aromatic carbon content) of the coke was completed in less than 2 hours in the drum.

Conclusions

The results indicated that the solid state ^{13}C NMR data were efective to evaluate the progress of the the coking process for the series of samples analysed. In all samples, the NMR data revealed an increase of aromaticity with the temperature and also an increase of the quaternary carbons. These results showed that the coking process was already completed in less than two hours of total residence time.

Acknowledgement. The authors acknowlwdge Dr. Luís Fernando Leite (PETROBRAS/CENPES/PROTER).

References

(1) Callejas, M.A.; Martínez, M. T.; Blasco, T.; and Sastre, E. P. - *Appl. Caalysis A*, **2001***, 218*, 181-188.
(2) Schabron, J. F.; Pauli, A. T.; Rovani, J.F.; Miknis, F. P.; *Fuel,* **2001**, 114.
(3) Saito, K. , Hatakeyama, M., Komaki, I., and Katoh, K.. *Journal Of Molecular Structure*; **2002**, 9, 602-603.

On-line determination of total sulfur in fuels

Rodney W. Spitler, Patrick J. Moore, and Rodney Friudenberg

Thermo ONIX
A Thermo Electron Business
9303 W. Sam Houston Parkway S.
Houston, TX 77099

Introduction

Environmental regulatory agencies, such as the U.S. E.P.A., are promulgating dramatic motor fuel sulfur level reductions. By 2006 the U.S. E.P.A requires the sulfur content of highway diesel to be reduced from 500 ppm S (w/w) to 15 ppm S (w/w).[1] The reduction of gasoline sulfur content is equally dramatic with the sulfur cap moving from 300 ppm S (w/w) to 80 ppm S (w/w) by 2006.[2] Reduction of motor fuel sulfur content is not isolated to the US. Sweden and Finland have had 10 ppm S (w/w) diesel for several years. Japan will require 50 ppm S (w/w) diesel by 2005 and Australia by 2006. Proposals being considered by the European Union may require < 10 ppm S (w/w) gasoline and diesel to be available by January 2005.[3] Latin American countries are also considering significant reductions in gasoline and diesel sulfur content. The challenge of meeting low sulfur fuel specifications is having a worldwide impact.

Low sulfur fuel specifications are presenting challenges to both refining and distribution. In the U.S., the low sulfur gasoline specifications, together with the expected elimination of MTBE, poses a new and potentially expensive challenge to gasoline blending operations. Should MTBE be eliminated as a gasoline additive the refiner will lose the use of a valuable gasoline diluent. Elimination of MTBE will increase the value of low sulfur gasoline blend components, such as, alkylate.[4] Distribution of refined motor fuels by pipelines presents yet another set of challenges. It is expected that 15 ppm S (w/w) diesel will necessarily be transported in a common pipeline system with 1,000 to 3,000 ppm S (w/w) distillates, such as, jet fuel. The opportunity for sulfur contamination of the 15 ppm S (w/w) diesel is enormous.[5] Rapid, precise and on-line determination of total sulfur will enable the economic operation of fuel blenders and provide a means for sulfur contamination detection in the fuel distribution system.

To meet these challenges, we have developed and validated a fully automated method for the on-line determination of total sulfur in diesel and gasoline. The method is similar to the well-accepted ASTM method D5453-00, "Determination of Total Sulfur in Light Hydrocarbons, Motor Fuels and Oils by Ultraviolet Fluorescence".[6] In our on-line method the sample is oxidized in an air atmosphere at 1100 °C. The oxidation process converts organic sulfur compounds and hydrogen sulfide to CO_2, H_2O and SO_2. The concentration of SO_2 in the oxidized sample is proportional to the total sulfur content of the fuel. Quantification of the SO_2 is accomplished with a pulsed ultra violet fluorescence, PUVF, spectrometer. Dominate applications for the on-line determination of total sulfur include: 1) detection of sulfur contamination in pipelines (pipeline transmix) and 2) fuel blending operations. In order to address these applications, particular attention was paid to response time and measurement precision during the development of our on-line method.

Experimental

Instrumentation. **Figure 1** is a simplified diagram of the instrumentation developed in this study. An automated liquid sample valve is used to pulse sample into the air bath oven at a typical rate of 2 µl/min. Air was selected as the carrier gas/oxidant over oxygen to ensure safe operation in potentially explosive atmospheres (the common installation environment for on-line analyzers). The air bath oven is typically held at 190 °C to ensure the complete vaporization of the sample. A mixing chamber is used to create a near constant flow of vaporized fuel and air to the combustion furnace. The combustion furnace is held at 1100 °C to ensure the complete oxidation of all sample components. Following oxidation a constant flow of analyte is presented to the PUVF spectrometer. The PUVF is selected for its superior sensitivity over ultraviolet fluorescence spectrometers with continuous UV light sources.

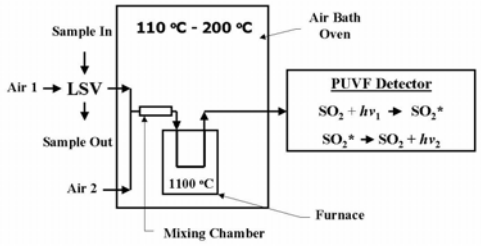

Figure 1. Simplified block diagram of instrumentation used for on-line determination of total sulfur in fuels.

Results and Discussion

Validation of Total Sulfur Measurement. Gasoline and diesel contain a wide variety of organic sulfur compounds plus potentially some hydrogen sulfide. Since approximately 90% of the gasoline pool sulfur comes from fluid catalytic cracked, FCC, gasoline, we examined its sulfur compound distribution.[7] FCC gasoline can contain thiophene, C_1-C_4 alkyl substituted thiophenes, benzothiophenes, tetrahydrothiophene, sulfides, disulfides and thiols.[8,9] To ensure that our on-line method fully accounts for all gasoline sulfur species a series of various sulfur compounds dissolved in iso-octane, toluene, hexane and benzene were analyzed as unknown samples. The instrument was calibrated with a thiophene in iso-octane standard prior to beginning these analyses. The purpose of these tests was to determine the conversion efficiency of the various sulfur compounds to SO_2 and to quantify errors, if any, resulting from dissimilar matrices. Results of this series of tests are presented in **Figure 2.** Examination of **Figure 2** indicates an ideal linear relationship between the reported and calculated total sulfur values, demonstrating a full accounting for the organic sulfur compounds tested. Additionally, one can conclude there is no aromatic matrix measurement error.

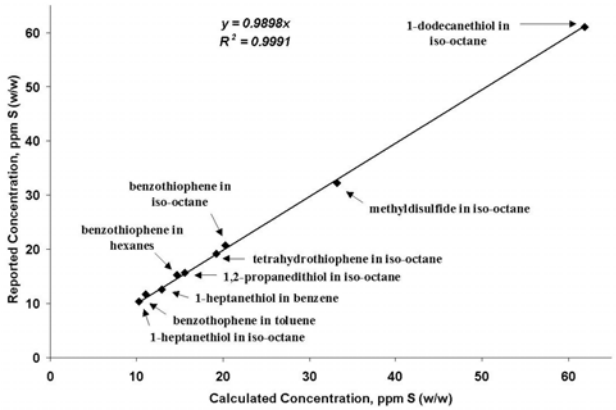

Figure 2. Reported vs. calculated values for gasoline range organic sulfur compounds in paraffinic and aromatic solvents.

Diesel fuel contains the same classes of sulfur compounds as gasoline, however, the sulfur compounds found in diesel will necessarily have higher boiling points than those found in gasoline.

Unlike gasoline, low sulfur diesel (≤ 15 ppm S (w/w)) can contain significant concentrations of refractory sulfur compounds, such as, dibenzothiophenes with alkyl substitutions at the 4 and 6 positions. Refractory sulfur compounds are difficult to remove by hydrotreating because steric hinderance prevents the sulfur atom from interacting with the catalytic site.[10,11] The response to various diesel range sulfur compounds were measured as described previously for gasoline range sulfur compounds, however, sulfur free (≤ 1 ppm S (w/w)) # 2 diesel fuel was used as the solvent. The results of this study are presented in **Figure 3**. **Figure 3** indicates an ideal linear relationship between the reported and calculated total sulfur values, demonstrating all sulfur compounds tested are fully converted to SO_2, including, the common refractory sulfur compound, 4,6-dimethyldibenzothiophene.

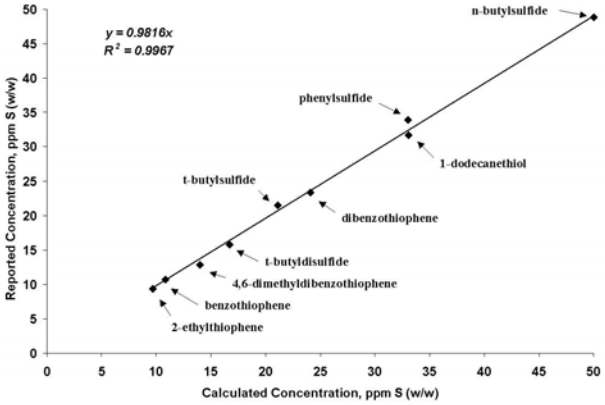

Figure 3. Reported vs. calculated values for diesel range organic sulfur compounds.

Measurement Linearity. Measurement linearity was evaluated for gasoline and diesel applications by preparing successive dilutions of thiophene in iso-octane and thiophene in # 2 diesel, respectively. **Figure 4** indicates excellent measurement linearity for thiophene in iso-octane from 4.98-99.60 ppm S (w/w) and thiophene in #2 diesel from 2.24-99.60 ppm S (w/w).

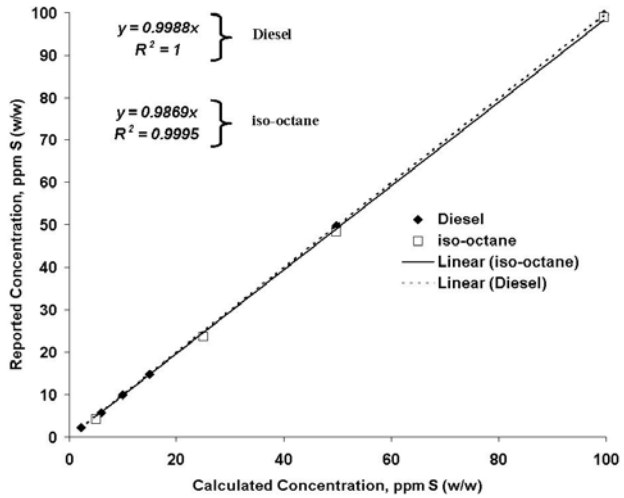

Figure 4. Thiophene in iso-octane and thiophene in #2 diesel measurement linearity.

Measurement Precision. Table 1 shows key statistics for a 14 hour run of a California gasoline and a 16 hour run of a Japanese diesel with mean sulfur concentrations of 4.01 ppm S (w/w) and 21.59 ppm S (w/w), respectively. More than 800 data points were collected for each measurement precision study. Excellent measurement precision is indicated for each fuel.

Table 1. Measurement Precision

Statistic	Gasoline 14 hr Run	Diesel 16 hr Run
Mean	4.01	21.59
Median	4.01	21.59
Mode	4.02	21.58
Standard Deviation	0.12	0.10
Range	0.79	0.66
Minimum	3.60	21.28
Maximum	4.38	21.93

Response Time. Response time was evaluated by switching between #2 diesel samples containing 22 ppm S (w/w) and 66 ppm S (w/w). The results of this test are summarized in **Figure 5**. As shown in **Figure 5** when switching from 22 ppm S (w/w) to 66 ppm S (w/w) approximately 1.0 minute is required to begin detecting the change in sulfur concentration. When switching from 66 ppm S (w/w) to 22 ppm S (w/w) approximately 1.5 minutes are required to begin detecting the change in sulfur concentration.

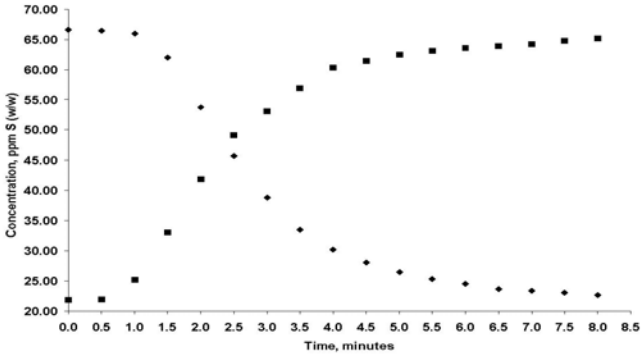

Figure 5. Response Time Measurements.

Conclusions

An on-line method for determination of total sulfur in gasoline and diesel was shown to provide an excellent linear accounting for gasoline and diesel range organic sulfur compounds at the lower expected future concentration requirements. The demonstrated response time of 1.0-1.5 minutes may be useful for detection of pipeline transmix, however, it is likely that improved response time would be valuable. The demonstrated measurement precision will allow this on-line method to be a valuable fuel blending control tool.

References

(1) *Federal Register,* **2000**, *66* (12), 5064.
(2) *Federal Register,* **2000**, *65* (28), 6754.
(3) Huss, A. In *Production of Low Sulfur Gasoline and Diesel Fuels*, Oral Presentation August **2002**.
(4) Barsamian, A. *World Refining* September **2001**, 30.
(5) Higgins, T. *World Refining* January/February **2002**, 4.
(6) *Annual Book of ASTM Standards* **2002**, Vol. 05.03, 446.
(7) Golden, S.; Fulton. S. *World Refining* July/August **2000**, 20.
(8) Shiraishi, Y.; Tachibana, K.; Taki, Y.; Hirai, T.; Komasawa, I. *Ind. Eng. Chem. Res.* **2001**, *40* (4), 1225.
(9) Albro, T.; Dreifuss, P.; Wormsbecher, R. *J. High Res. Chrom.* **1993**, *16*, 13.
(10) Rodgers, R.; White, F.; Hendrickson, C.; Marshall, A; Andersen, K. *Anal. Chem.* **1998**, *70* (22), 4743.
(11) Isoda, T.; Nagao, S.; Ma, X.; Korai, Y; Mochida, I.; *Energy Fuels* **1996**, *10* (2), 482.

Solvent and Matrix Effects in the Mass Spectrometric Analysis of Polyaromatic Sulfur Compounds in the Presence of Palladium (II)

Walter E. Rudzinski, Xuemei Luo

Department of Chemistry
Southwest Texas State University
San Marcos Tx, 78666

Introduction

The nucleophilic interaction of sulfur compounds with $PdCl_2$ to form complexes has been well documented in the literature,[1-6] and the interaction has been exploited for the ligand exchange chromatography (LEC) of polyaromatic sulfur heterocycles (PASH). There are however some deficiencies in the LEC method: organosulfur compounds elute as $PdCl_2$ complexes, benzothiophenes are not completely recovered, and constituents with a terminal (as opposed to an internal) thiophene ring elute early.[7] In addition, the affinity of the $PdCl_2$ varies with the organosulfur ring size and decreases in the order 3-ring> 2-ring> 1-ring PASH. [3,7] The results seem to indicate that the goal of a general chromatographic method for the separation of polyaromatic sulfur heterocycles (PASH) remains elusive.

An alternative approach for the separation of PASH compounds involves mass spectrometry. As recently reported, a redox reaction can occur between Pd(II) and PASH compounds in the electrospray ionization source of a mass spectrometer.[8] The reaction yields PASH radical cations which are easily identified and quantified. We now report significant improvements to the sensitivity, and limit of detection for the method when using a (50:50) methanol: dichloromethane solvent mix, as well as the selectivity of the method when detecting PASH compounds in a hydrogenated oil matrix. The applications of chromatography and mass spectrometry to petroleum analysis have recently been reviewed.[9-11]

Experimental

Reagents and Chemicals. Methanol (CH_3OH), acetonitrile (CH_3CN), dichloromethane (CH_2Cl_2), and hexane were all chromatographic grade and obtained from EM Science (Gibbstown, NJ); $PdCl_2$ and the organosulfur compounds: dibenzothiophene (DBT), thianthrene (TAN), benzonaphthothiophene (BNTP), 4,6-dimethyl-dibenzothiophene (4,6-DBT) and 2-methyl dibenzothiophene (2-DBT) were obtained from Sigma-Aldrich (Milwaukee, WI). Hydrogenated oil was obtained from Exxon-Mobil.

Preparation of Samples. PASH stock solutions were prepared as either 10mM or 1 mM (TAN) solutions in either (50:50) CH_3OH: CH_3CN or CH_2Cl_2. A 20 mM $PdCl_2$ stock solution was prepared either in (50:50) CH_3OH: CH_3CN or CH_3CN. The hydrogenated oil was dissolved in hexane to a final concentration of 100 mg/mL.

PASH mixture #1 was prepared by taking a 1-20 µl aliquot of the appropriate compound in (50:50) CH_3OH: CH_3CN then diluting to 1 mL in (50:50) CH_3OH: CH_3CN to the following concentrations: $1.5x10^{-4}$ M TAN, $1x10^{-3}$M DBT, $1x10^{-3}$M 2-DBT, $1x10^{-3}$M 4,6-DBT, $2x10^{-3}$M BNTP and 2 - 4 mM $PdCl_2$.

PASH mixture #2 was prepared by taking the appropriate PASH in CH_2Cl_2 then diluting to 1 mL in (50:50) CH_3OH: CH_2Cl_2 to the following concentrations: $1x10^{-6}$M TAN, $5x10^{-4}$M DBT, $1x10^{-4}$ M 2-DBT, $2x10^{-5}$M 4,6-DBT, $5x10^{-5}$M BNTP and 0.5 - 1 mM $PdCl_2$.

PASH mixture #3 in hydrogenated oil was prepared by taking an appropriate aliquot of PASH in CH_2Cl_2, $PdCl_2$ in CH_3CN, and hydrogenated oil in hexane then diluting to 1 mL in (50:50) CH_3OH: CH_2Cl_2: to the following concentrations: $1x10^{-6}$M TAN, $5x10^{-4}$M DBT, $1x10^{-4}$ M 2-DBT, $2x10^{-5}$M 4,6-DBT, $5x10^{-5}$M BNTP, 0.5 - 1 mM $PdCl_2$ and 10mg/mL hydrogenated oil.

Instrumentation. Mass spectra were obtained on a Finnigan LCQ ion trap mass spectrometer (MS) equipped with an electrospray ionization (ESI) source. Excalibur software, version 1.2 (Finnigan Corp., 2000) was used for data acquisition and plotting.

Instrumental parameters used with the ESI ionization source and Finnigan LCQ were as follows: nitrogen sheath gas pressure, 80psi; nitrogen sheath gas flow rate, 60 (arbitrary units); positive ion mode; ion spray voltage, 3.5kV; capillary temperature, 200°C; capillary voltage, 60V; tube lens offset voltage, 40V. Each MS scan was based on the average of 5 microscans and MS spectra were averaged based on at least 25 scans.

The samples were introduced by direct infusion at a flow rate of 2µl/min.

Results and Discussion.

The limit of detection (LOD) was determined both in the (50:50) CH_3OH: CH_3CN and (50:50) CH_3OH: CH_2Cl_2 binary solvent mixtures using the formula, LOD = 3s/m where s is the average background noise and m is the response/ molar concentration. The results are presented in Table 1 which clearly show a lowering of the LOD in (50:50) CH_3OH: CH_2Cl_2 by a factor of 150 or more for TAN, 4,6-DBT and BNTP, 18 for 2-DBT and 5 for DBT. As previously intimated by Van Berkel and coworkers, this result is probably due to the increased stabilization of radical cations in CH_2Cl_2. [12]

Table 1. Limit of Detection for PASH Compounds

Compounds	LOD in CH_3OH: CH_2Cl_2 (50:50)	LOD in CH_3OH: CH_3CN (50:50)
TAN	3.0×10^{-7}M	4.5×10^{-5}M
DBT	1.8×10^{-4}M	9.0×10^{-4}M
2-DBT	5.0×10^{-5}M	9.0×10^{-4}M
4,6-DBT	7.5×10^{-6}M	4.5×10^{-3}M
BNTP	1.8×10^{-5}M	4.5×10^{-3}M

Figure 1 shows the mass spectrometric results obtained for several samples in the (50:50) CH_3OH: CH_2Cl_2 binary solvent mixture.

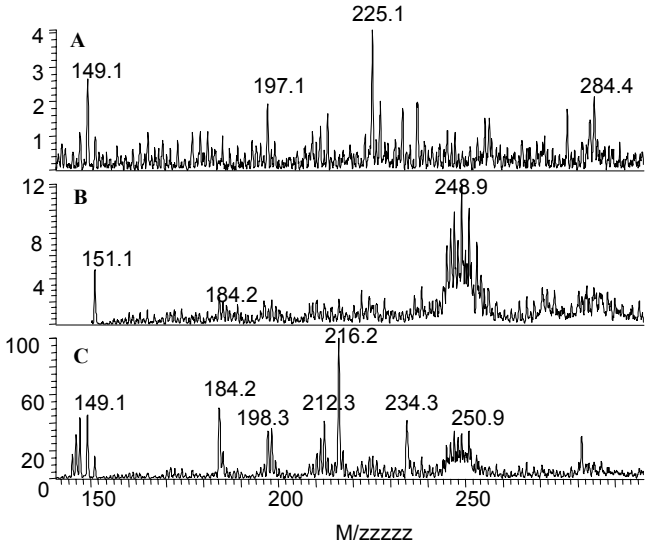

Figure 1. Mass Spectrometric response for: (A) 10 mM hydrogenated oil; (B) 10 mM hydrogenated oil and 0.5 mM $PdCl_2$; (C) mixture #3 which consists of TAN, DBT, 2-DBT, 4,6-DBT, BNTP, $PdCl_2$ and hydrogenated oil.

Figure 1 (A) clearly illustrates that the matrix, the hydrogenated oil, does not generate many peaks and those which are present generate minimal response (less than 4). Figure 1B illustrates the response for a mixture of the hydrogenated oil and $PdCl_2$. A broad envelope is centered about an m/z of 249 which is attributed to a palladium cluster. Figure 1C illustrates the response of the hydrogenated oil, $PdCl_2$ and PASH mixture that clearly shows peaks which can be attributed to DBT (184), 2-DBT (198), 4,6-DBT (212), TAN (216), and BNTP (234). The m/z ratio of the radical cation is in parentheses following the acronym of the PASH.

Conclusions

The mass spectrometric results clearly indicate that PASH compounds in the presence of $PdCl_2$ in (50:50) CH_3OH: CH_2Cl_2 give an enhanced response even in the presence of a hydrogenated oil. Further work is now in progress to extend the approach to complicated crude oils.

Acknowledgement. WER would like to thank the Environmental Protection Agency (Grant No.R825503) and the Texas Higher Education Coordinating Board through the Advanced Technology Program (ATP) for support of this project. WER would also like to thank the Institute for Industrial and Environmental Science of Southwest Texas State University and Exxon Mobil for donation of the hydrogenated oil.

References

1. Nishioka, M. *Energy Fuels,* **1988**, *2,* 214-219.
2. Later, D.W.; Lee, M.L.; Bartle, K.D.; Kong, R.C.; Vassilaros, D.L., *Anal. Chem*., **1981**, *53*, 1612-1620.
3. Milenkovic, A.; Schultz, E.; Meille, V.; Loffreda, D.; Forissier, M.; Vrinat, M.; Sautet, P.; Lemaire, M., *Energy Fuels*, **1999**, *13,* 881-887.
4. Wright, B.W.; Peaden, P.A.; Lee, M.L.; Stark, T., *J. Chromatogr*., **1982**, *248,* 17-34.
5. Grang, B.Y., *Anal. Lett.* **1985**, *18,* 193-202.
6. Nishioka, M.; Campbell, R.M.; Lee, M.L.; Castle, R.N., *Fuel* **1986**, *65*, 270 - 273.
7. Rudzinski, W.E.; Sassman, S.; Watkins, L.M., *Prepr.- Am. Chem. Soc. , Div. Petr. Chem.,* **2000**, *45(4)*, 564-566.
8. Rudzinski, W.E.; Zhang, Y.; Luo X., *J. Mass Spec.*, **2003**, in press.
9. Mansfield, C.T.; Barman, B.N.; Thomas, J.V.; Mehrotra, A.K.; McCann, J.M., *Anal. Chem.*, **1999**, *71*, 81R-107R.
10. Barman, B.N., Cebolla, V.L., Membrado, L., *Crit. Rev. Anal. Chem.,* **2000**, *30*, 75-120
11. Rudzinski, W.E., In *Analytical Advances in Hydrocarbon Research*, C. Hsu ed, Kluwer Academic: New York, N.Y., **2003** in press.
12. Van Berkel G.J.; Kertesz, V., *J. Mass Spectrom*., **2001**, 36, 1125-1132.

Petroleomics: Electrospray ionization FT-ICR mass analysis of NSO compounds for correlation between total acid number, corrosivity, and elemental composition

Geoffrey C. Klein[a], Ryan P. Rodgers[b], Marco A.G. Teixeira[c], Ana Maria R. F. Teixeira[d], and Alan G. Marshall[b]

[a]Department of Chemistry and Biochemistry, Florida State University, Tallahassee, FL 32306
[b]Ion Cyclotron Resonance Program, Florida State University, National High Magnetic Field Laboratory,1800 East Paul Dirac Drive, Tallahassee, FL 32310-3706
[c]Petrobras R&D Center/Chemistry, Cidade Universitaria, Rio de Janeiro, Brazil EEP 21949-900
[d]Fluminense Federal University-GQA, Outeiro do Valonguinho, s/n, Niteroi, RJ, Brazil

Introduction

Hughey et. al. recently reported the assignment of elemental composition of NSO compounds by microelectrospray Fourier transform ion cyclotron resonance (FT-ICR) mass spectrometry.[1] Electrospray selectively ionizes the polar compounds and FT-ICR MS provides the high resolution (> 100,000) and high mass accuracy (< 1 ppm) needed to resolve and identify thousands of components in a complex mixture. Polar compounds, containing N-, S-, and O- (<15% of crude composition), are critically important in refining.[2] For example, heteroatom-containing hydrocarbons, particularly those containing nitrogen, are known to play a key role in catalyst deactivation through coke formation on the catalyst surface. Similarly, naphthenic acids are known to cause process corrosion in refining equipment. Here, we try to correlate total acid number (TAN), corrosivity, and elemental composition within crude oils.

Experimental

Oil samples. Ten crude oils exhibiting different total acid number (TAN) and corrosivity, provided by Petrobras, are shown in Table 1. TAN was determined by the amount of KOH needed to neutralize one gram of crude oil. A wire probe composed of the same material as refining equipment is placed in the stream of the crude oil. Decay (and therefore a measure of process corrosion) of the wire is detected by changes in wire resistance. Corrosive character was assigned by a team of specialists based on this wire test, field data, and their expertise.

Table 1. Crude oils analyzed

Crude Oil	TAN	Corrosivity
A1	4.0	High
A2	2.3	High
A3	1.8	High
A4	1.5	High
A5	0.3	High
B1	1.0	Medium
B2	0.5	Medium
B3	0.5	Medium
C1	0.8	Negligible
C2	0.3	Negligible

Sample Preparation. 20 mg of the crude was dissolved in 3 mL of toluene, and then diluted to 20 mL with methanol. 1 mL of the final solution was spiked with either 3 μL of acetic acid or 10 μL of ammonium hydroxide to facilitate protonation (+ ion ESI) or deprotonation (- ion ESI). All mass spectra were collected by both positive- and/or negative-ion electrospray (ESI) with a homebuilt 9.4 T FT-ICR mass spectrometer.[3] Spectra were externally calibrated from #G2421A electrospray "tuning mix" from Agilent, and then recalibrated from a homologous series within each crude oil.

Data analysis. Analysis was performed by convertion of IUPAC measured mass to the Kendrick mass scale (CH_2 = 14.00000 instead of 14.01565 Da) to facilitate identification of homologous series. Kendrick mass is obtained by multiplying the IUPAC mass with 14/14.0156. The advantage to the Kendrick mass scale is that the members of a single homologous series (compounds with the same heteroatomic composition and number of rings and double bonds, but differ by a CH_2 group) have identical Kendrick mass defect (KMD), seen in Eq. (1),

$$\text{KMD} = (\text{Nominal Kendrick Mass} - \text{Kendrick Mass}) \qquad (1)$$

where nominal Kendrick mass is determined by rounding up the Kendrick mass to the nearest whole number. Series are then separated based on even and odd nominal Kendrick mass and KMD as described elsewhere.[4]

Results and Discussion

Figure 1 shows compositional data and O_2/N ratio for all ten crude oils. This ratio was determined by summing the relative abundance of all compounds that contain O_2 (representing a carboxylic acid) divided by the sum of relative abundances for neutral nitrogen compounds. A higher ratio may indicate a higher abundance of carboxylic acids that are known to contribute to the corrosion of refining equipment. Some of the carboxylic acids contained more than one heteroatomic atom, such as in crude oil A2 and C2, which contains a high abundance of NO_2-species. This ratio is not the only clue to the corrosivity, as evident by A3, which contains high corrosivity (by wire measure) contains a low O_2/N ratio.

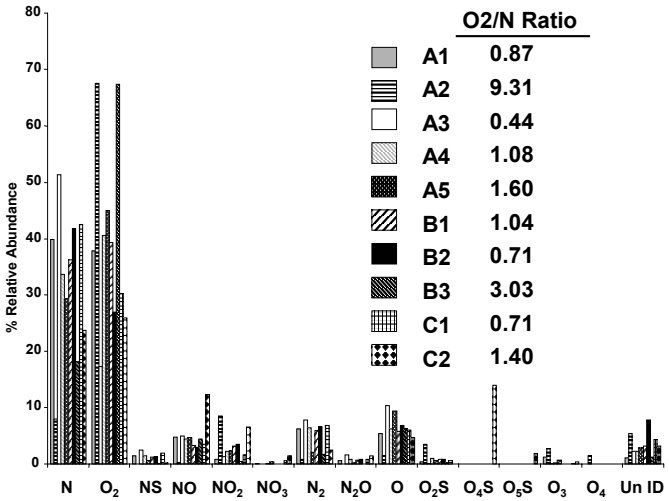

Figure 1. Comparison of compound classes in negative-ion mode microelectrospray FT-ICR MS for each crude oil. Only those classes with relative abundance > 1% are shown.

Carboxylic acids found in the ten crude oils are composed of naphthenic acids (containing 1-3 rings and double bonds) and a variety of aromatic acids, from mono-aromatic to hexa-aromatic. **Figure 2** shows the distribution of rings and double bonds found in the O_2- species in the crude oils. The composition of the carboxylic acids was determined by summing the relative abundance of each

acid and dividing by the total relative abundance of all compounds present in the crude oil. For 9 out of 10 crude oils (all except B2), the relative abundance of the naphthenic acids is higher than all other components found in the O_2-species. The relative abundance of naphthenic acids tends to be higher for crude oils exhibiting high corrosive character. This is not true for all oils. B3 has the highest naphthenic relative abundance but only exhibits medium corrosivity; however, it contains a TAN value of 0.5, which is still considered acidic. Surprisingly, A3 has the second lowest naphthenic acid relative abundance but exhibits high corrosivity and a TAN value of 1.8. This suggests that NSO polar compounds may not be the only components of crude oils that contribute to process corrosivity.

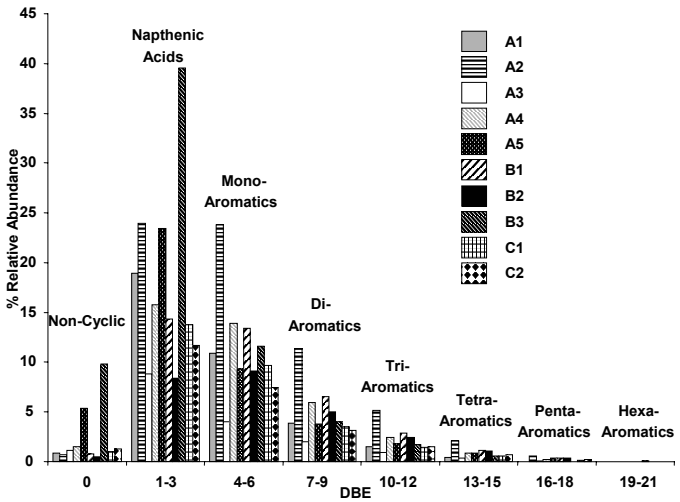

Figure 2. Comparison of the distribution of double bond equivalence (DBE) in O_2-species, where DBE is the number of rings and double bonds.

Petroleum acids are found in predominantly immature, biodegraded, and heavy crudes.[5] Higher corrosive crudes should exhibit a smaller carbon number distribution than lower corrosive crudes. **Figure** 3 shows the carbon distribution of 4 DBE O-series for 4 crude oils with different corrosive character. The two oils

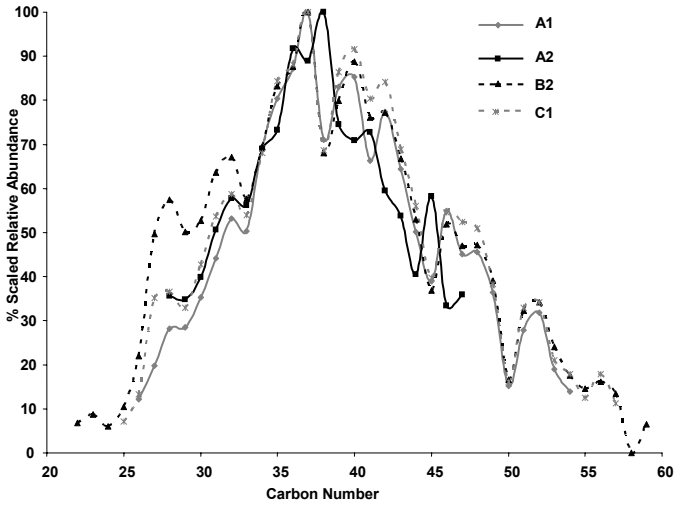

Figure 3. Distribution of Carbon in O-series (Phenol) with 4 rings or double bonds.

with high corrosivity have a carbon number distribution of 26-54 and 28-47, while the less corrosive crudes have distributions from 22-59 and 25-57 carbons. The slightly smaller carbon distribution of the high corrosive crudes suggests that the compounds have undergone a higher degree of biodegradation.

Positive-ion spectra were collected for three of the crude oils to determine the effect of the basic compounds on corrosivity and TAN. **Figure 4** clearly illustrates that the basic nitrogen compounds do not affect the components found in negative-ion mode. All three crude oils are composed of ~ 83% basic nitrogen species, with comparable carbon number distributions and rings and double bonds.

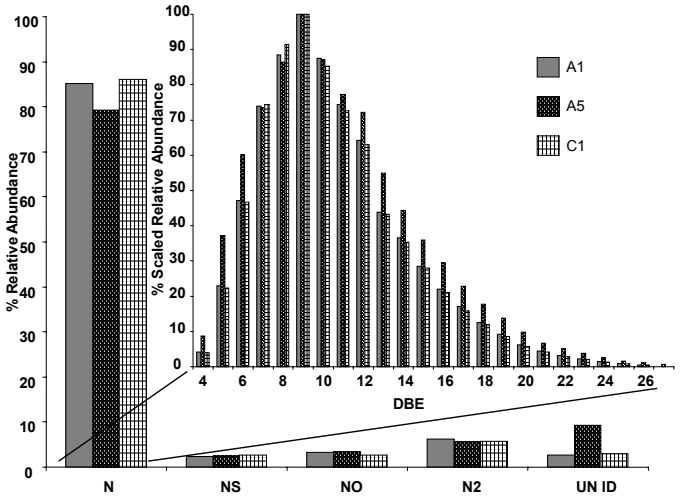

Figure 4. Comparison of compounds classes and double bond equivalence for N-series identified in positive-ion mode for 3 crude oils.

Conclusions

FT-ICR MS provides the necessary mass resolving power and mass accuracy (<1ppm) to assign elemental composition to the NSO compounds found by negative-ion microelectrospray. Our results suggest that these polar compounds are not the only components contributing to the process corrosivity of crude oils, but can provide helpful clues. A higher ratio of O_2/N species, a higher relative abundance of naphthenic acids and a smaller distribution of carbon number may indicate that a crude oil exhibits higher corrosive character. Positive spectra were also collected and determined that the basic components identified do not play a role in the correlation of TAN, corrosivity and elemental composition.

Acknowledgement. The authors would like to thank Daniel MacIntosh for machining all of the custom parts required for the 9.4T instrument construction. This work was supported by NSF (CHE-99-09502), Florida State University, Petrobras, and the National High Magnetic Field Laboratory.

References

(1) Hughey, H. A.; Rodgers, R. P.; Marshall, A. G.; Qian, K.; and Winston, K. R. *Org. Geochem.*, **2002**, 33 (7), 743.
(2) Altgelt, K. H., Boduszynski, M.M. In *Composition and Analysis of Heavy Petroleum Fractions*; Marcel Dekker: New York, 1994; pp 393-484.
(3) Senko, M.W.; Hendrickson, C. L.; Pasa-Tolic, L.; Marto, J. A.; White, f. M.; Guan, S.; Marshall, A. G. *Rapid Commun. Mass Spectrom.* **1996**, 10, 1824.
(4) Hsu, C.S.; Qian, K.; Chen, Y.C. *Anal. Chim. Act.* **1992**, *264*, 79.
(5) Ahsan, A.; Karlsen, D. A.; Patience, R. L. *Mar. Pet. Geol.* **1997**, 14, 55.

THE POTENTIAL OF HYPY-GC-MS FOR FINGERPRINTING PETROLEUM SOURCE ROCKS AND COALS

Colin E. Snape[1]*, William Meredith*[1]*, Christopher A Russell*[1]*, Mick Cooper*[1]*, Gordon D. Love*[2] *and Daniele Fabbri*[3]

[1]Nottingham Fuel and Energy Centre, School of Chemical, Environmental and Mining Engineering, University of Nottingham, University Park, Nottingham NG7 2RD, UK
[2]School of Civil Engineering and Geosciences, Drummond Building, The University, Newcastle upon Tyne NE1 7RU, UK
[3]Laboratorio di Chimica Ambientale, Università di Bologna, via Marconi 2, 48100 Ravenna, Italy

Introduction

The use of hydropyrolysis (commonly abbreviated to *hypy*), which refers to pyrolysis assisted by high hydrogen gas pressures (>10 MPa) in the presence of a dispersed catalyst, as an analytical pyrolysis method for liberating covalently-bound biomarker hydrocarbon structures from kerogen was first reported by Love *et al.*(1). This and other subsequent studies have demonstrated the unique capability of the fixed-bed catalytic hydropyrolysis procedure to release much higher yields of aliphatic biomarker hydrocarbons (including *n*-hydrocarbons, hopanes, steranes and methyl steranes) from immature kerogens compared to mild catalytic hydrogenation and traditional pyrolysis methods(1-5). These characteristics allow for the bound biomarkers released by hydropyrolysis to offer potential solutions to tackling many problems in oil exploration, especially where the conventional geochemical approach using the free (extractable) hydrocarbon biomarkers cannot be employed, such as for severely biodegraded oils and samples contaminated with oil based drilling muds.

Although pyrolysis-GC-MS is widely used as a fingerprinting technique for sedimentary organic matter(6-9) and also for other materials, notably polymers, the inherent low yields limit the application of the technique to the more thermally labile moieties in kerogens. Thus, if hydropyrolysis can be interfaced with GC-MS (hypy-thermal desorption-GC-MS), this new development should have considerable commercial potential as a superior technique for rapid characterisation of all macromolecular substances. This study describes the development of an experimental procedure in which product oils are trapped on silica to facilitate analysis by thermal desorption GC-MS without any prior work-up.

Experimental

Samples Göynük oil shale (GOS) was used to assess the capability of the silica-filled trap for recovering hydropyrolysis product oil. This lacustrine oil shale of Tertiary age has been classified as a type I kerogen, and characterised previously (Love et al., 1997). It was pre-extracted with DCM/methanol (93:7 v/v), washed with dilute HCl (2M) at 50ºC for 3 hours and re-extracted with DCM/methanol (93:7 v/v), so any products generated will be predominantly released from the kerogen phase.

Hydropyrolysis Fixed bed hydropyrolysis was conducted using the apparatus and procedure that have been described in detail elsewhere (Snape et al., 1989; Lafferty et al., 1993; Love et al., 1995). Briefly, the samples were pyrolysed with resistive heating from 50°C to 250°C at 300°C min^{-1}, and then from 250°C to 500°C at 8°C min^{-1}, under a hydrogen pressure of 15 MPa. A hydrogen sweep gas flow of 10 dm^3 min^{-1}, measured at ambient temperature and pressure ensured that the products were quickly removed from the reactor vessel. As in previous studies, the hydropyrolysates were recovered with multiple washes of DCM from the dry ice cooled trap, which consisted of coils of ⅜" stainless steel. These results could then be compared to those obtained with the hydropyrolysates collected in the silica filled trap constructed from ¼" stainless steel (0.180" i.d.), and designed to hold approximately 0.75 g of silica. To ensure that there was no contamination of the products, the silica used for trapping (35-70 mesh) was pre-extracted in a soxhlet with *n*-hexane for 24 hours and DCM/methanol (93:7 v/v) for 48 hours, and dried in a baffle furnace at 600°C for 4 hours.

In order to quantitatively assess the recoveries of hydrocarbons by hydropyrolysis, aliquots (~50 mg) of a light crude oil were adsorbed to a small amount of silica and pyrolysed. The desorbed oils were recovered from each of the two designs of trap, cooled by both dry ice and with liquid nitrogen. The temperature within the silica trap was measured by inserting a thermocouple into the trap at the base of the silica column during a blank run with each of the two coolants. Quantification of the recovered hydrocarbons (DCM soluble fraction) was achieved by the addition of squalane, with analysis by gas chromatography-flame ionisation detection (GC-FID).

The aliphatic hydrocarbon, aromatic hydrocarbon and polar (NSO) fractions of the oil shale and asphaltene hydropyrolysates were separated by silica gel adsorption chromatography with successive elutions of *n*-hexane, *n*-hexane/DCM (4:1 v/v) and DCM/methanol (1:1 v/v). The yields of each fraction were determined by evaporation under a stream of dry nitrogen in pre-weighed vials. In order to assess the degree of carbon conversion during hydropyrolysis, and the yield of carbon recovered, the carbon content of the samples, pyrolysis residues, hydropyrolysates and desorption residues were determined with a UCI Coulometrics CO_2 coulometer.

Thermal desorption of hypy oils The off-line thermal desorption of the silica trapped hydropyrolysis products of the GOS were performed in the hydropyrolysis reactor under an atmospheric pressure of hydrogen with a sweep gas flow of 100 cm^3 min^{-1}, measured at ambient temperature. The samples were desorbed with a heating rate of 50°C to 300°C at 300°C min^{-1}, with the final temperature held for 2 mins. The desorbed products were then trapped on silica as for the hydropyrolysis experiments. Further tests were carried out to a maximum temperature of 350, 400, 450 and 500°C, at the same heating rate, with the final temperature again held for 2 mins. The on-line thermal desorption-GC-MS of the silica trapped hydropyrolysis oils were performed Pyrolysis experiments were performed using a CDS 1000 pyroprobe platinum heated filament pyrolyser (Chemical Data System, Oxford, USA) directly connected to a Varian 3400 gas chromatograph coupled to a Varian Saturn II ion trap mass spectrometer. The Py/GC interface and the split/splitless Varian 1077 injector (at split ratio 30:1) were kept at 280°C. Silica trapped sample (about 5 mg) and Göynük oil (about 0.2 mg) were pyrolysed at 700°C (set temperature) for 10 sec at the maximum heating rate. The solution containing aliphatic fraction was analysed by direct injection into the GC-MS apparatus using the above described conditions.

Results and Discussion

Comparison of coiled trap and silica The recovery of the light crude oil desorbed by hydropyrolysis is illustrated in Fig. 1. The whole oil gas chromatogram (Fig. 1A) is dominated by a homologous series of *n*-alkanes (nC_7 to nC_{32}), and low molecular weight aromatic compounds such as benzene and toluene. Table 1 summarises information on the recovery of the light oil for the two

types of trap, using the different coolants. It can be seen that for the relatively high molecular mass alkanes (>nC$_{10}$), both the normal coiled trap and silica are very efficient (generally >80% w/w), with no significant differences between the two coolants. Major differences in recovery are only apparent for the relatively low molecular weight compounds (<nC$_{10}$), and so the trapping efficiency of biomarker hydrocarbons (>nC$_{20}$) should be equally as good for the silica trap as for the coiled steel design. Therefore, the recovered DCM soluble oil fractions (Figs. 1B & 1C) are illustrated as partial gas chromatograms showing only the distribution of the low molecular weight compounds.

Table 1. Recovery (% w/w) of selected hydrocarbons desorbed from a light crude oil under hydropyrolysis conditions.

Compound	Coiled trap		Silica trap	
	Liquid N_2	Dry ice	Liquid N_2	Dry ice
Benzene	58	0	43	0
nC$_7$	58	0	46	0
Toluene	83	52	83	37
nC$_8$	79	51	77	4
nC$_9$	83	75	85	84
nC$_{10}$	87	83	97	88
nC$_{11}$	89	87	96	89
nC$_{12}$	89	88	91	91
nC$_{13}$	91	90	87	94
nC$_{14}$	97	95	99	98
nC$_{15}$	96	93	102	96
nC$_{20}$	86	88	92	92
nC$_{25}$	81	85	78	89
nC$_{30}$	77	94	81	88

The use of liquid nitrogen as the coolant in place of dry ice resulted in a significantly enhanced recovery of low molecular weight compounds such as the nC$_7$ and nC$_8$ alkanes, benzene and toluene. The recovery of these compounds was slightly greater from the coiled steel trap cooled with liquid nitrogen than from the silica filled trap. The higher recovery from the coiled steel trap was more significant with dry ice as the coolant, with just 4% w/w of the nC$_8$ alkane and 37% w/w of the toluene recovered from silica trap, compared to 51% and 52% w/w respectively recovered from the coiled steel trap.

Due to its much lower temperature (-196ºC), the liquid nitrogen should be a much more efficient coolant than the solid dry ice (-78ºC). However, the liquid nitrogen tended to quickly evaporate during the course of the run as the hot sweep gas warmed the trap. Therefore, the temperature at the base of the trap rose steadily from -130ºC when the reactor was at 300ºC, to 85ºC at the end of the test. This was similar to the final temperature observed when dry ice was used as the coolant (65ºC), and might have caused some of the low molecular weight compounds to evaporate and be swept out of the trap.

Information on the efficiency of the different designs of trap in recovering the hydropyrolysate generated by the hydropyrolysis of GOS is presented in Table 2. As in previous studies on this shale, hydropyrolysis resulted in carbon conversions of >90%, with relatively high yields of the GC amenable aliphatic and aromatic hydrocarbons generated. The errors of these analyses are estimated at ±5% based on previous described repeat analyses (Love et al., 1995). The efficiencies of the traps are expressed as the % of the converted carbon, and the wt. % of the total products recovered in each type, and show that the silica-filled and coiled steel traps recover a very similar proportion of the converted organic carbon, principally as DCM-soluble products. These recovery figures may be a slight underestimation of the true values, due to evaporative losses, inevitable while removing the excess DCM to obtain the total hydropyrolysate yield.

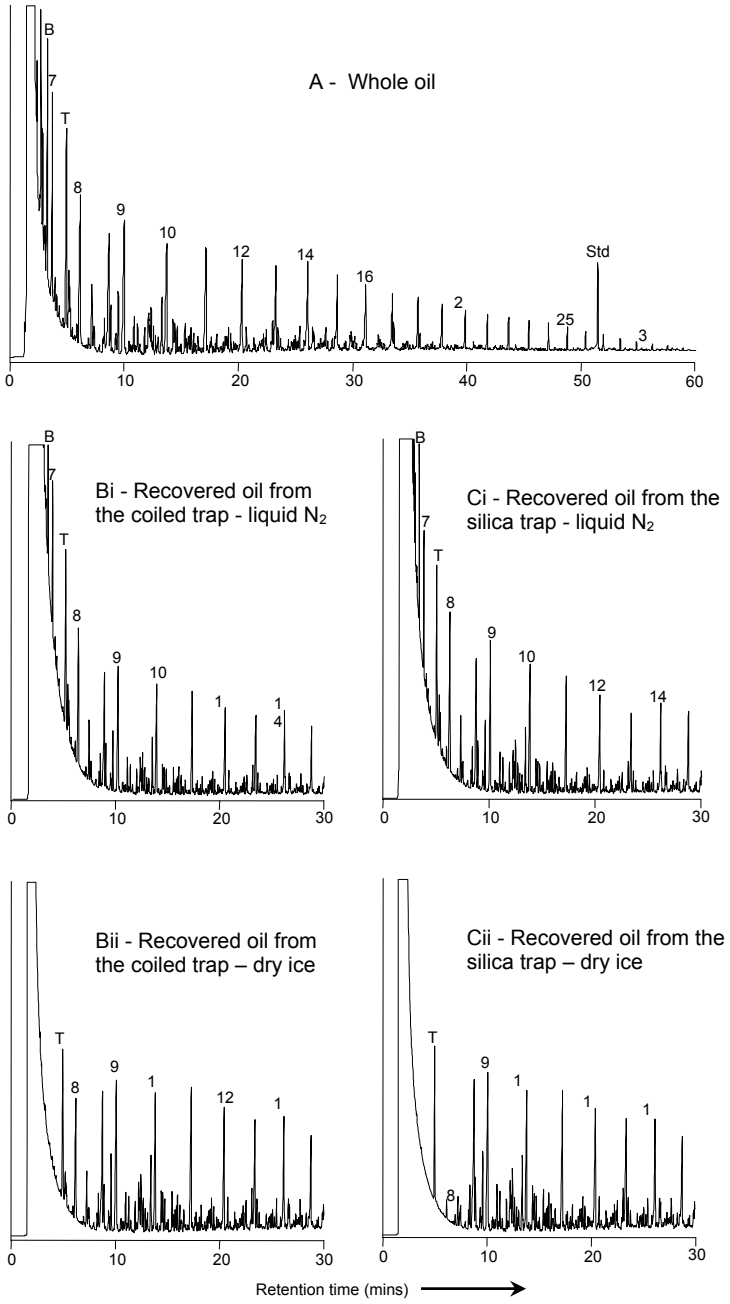

Figure 1. Comparison of the whole oil gas chromatogram (A), and the partial gas chromatograms of the DCM-soluble fraction desorbed by the hydropyrolysis of a light crude oil, with trapping by the coiled steel (B) and silica filled trap (C), cooled by liquid nitrogen (i) and dry ice (ii). Numbers refer to the carbon number of the n-alkanes; B - Benzene; T - toluene; Std - squalane.

The distribution of the GOS hydropyrolysate throughout the trap silica column is presented in Table 3. The results for each section are expressed as the wt. % of each fraction present, together

with the proportion of carbon recovered. The vast majority of the hydropyrolysate is adsorbed to the upper quarter section, with >70% w/w of each fraction, and of the total carbon in this section. There is then a rapid decrease in the proportion of hydropyrolysate adsorbed to the middle sections, with <5% w/w present in the lower silica section. These results indicate that providing sufficient silica is present in the trap for the mass of carbon generated from the sample, no significant quantities of the product, other than highly volatile compounds, should pass through the trap without adsorbing to the silica.

Table 2. Comparison of the results obtained from the hydropyrolysis of the Göynük oil shale with the different trapping methods.

	Coiled trap	Silica trap
Sample weight (mg)	100	50
Trap silica weight (g)	-	1.0
Carbon conversion (% initial TOC)[a]	91.2	93.0
Trapping efficiency (% TOC generated)[b]	91.5	94.5
Trapping efficiency (wt. % of products)[c]	80.0	80.9
Yield of aliphatics (mg/g initial TOC)[d]	159	175
Yield of aromatics (mg/g initial TOC)[e]	89	101
Yield of total oil (mg/g initial TOC)[f]	1110	1200

[a] % TOC removed from sample by hydropyrolysis. [b] % of generated TOC recovered. [c] % of sample weight loss recovered as DCM soluble product oil. [d] Weight of recovered aliphatic fraction (mg) / weight of initial TOC (g). [e] Weight of recovered aromatic fraction (mg) / weight of initial TOC (g). [f] Total weight of recovered DCM soluble product oil (mg) / weight of initial TOC (g).

Table 3. Distribution of the hydropyrolysate fractions (wt. %) and TOC (%) throughout the silica column containing the hydropyrolysate of the Göynük oil shale.

Silica section	% Aliphatic	% Aromatic	% Polar	% TOC
Upper	80	71	70	73
Upper middle	13	16	18	15
Lower middle	5	8	7	8
Lower	2	5	5	4

Table 4. Selected aliphatic biomarker maturity parameters from the hydropyrolysate of the Göynük oil shale.

Ratio	Coiled trap	Silica trap	
		All silica	Top section
C31αβ(22S/S+R)[a]	0.21	0.18	0.18
C32αβ(22S/S+R)[b]	0.14	0.12	0.14
C30βα/αβ[c]	1.97	2.03	2.02
Ts/Tm[d]	0.29	0.29	0.32
C29ααα(20S/S+R)[e]	0.05	0.05	0.05
C29αββ/ααα+αββ[f]	0.27	0.25	0.27

[a] αβ-homohopane 22S / S + R - starting value 0, ratios reach end point at 0.6 before the onset of intense oil generation. [b] C_{32} αβ-dihomohopane 22S / S + R - as ratio [a]. [c] C_{30} βα-moretane / C_{30} αβ-hopane - ratio decreases with increasing maturity. [d] 18α,21β(H-22,29,30-trisnorneohopane / 17α,21β(H)-22,29,30-trisnorhopane - ratio increases with increasing maturity. [e] C_{29} ααα-ethylcholestane 20S / S + R - increases to 0.5 with increasing maturity. [f] C_{29} ethylcholestane αββ / ααα + αββ – increases to 0.8 with increasing maturity.

In addition to the total yield of hydropyrolysate recovered, it is also important that the silica-filled trap produces biomarker hydrocarbon profiles similar to those obtained from the coiled steel trap. A number of maturity dependant biomarker ratios based on the abundance of individual isomers are listed in Table 4, and indicate that the composition of the hydropyrolysates recovered from the silica-filled traps are very similar to those from the coiled steel trap. In addition, it can be seen that the top section of the silica column, which as described contains the highest concentration of hydropyrolysate is representative of the silica column as a whole. This has implications for the on-line thermal desorption py-GC-MS of the silica trapped hydropyrolysis oil described below as only a small amount of the total silica recovered from the trap can be introduced to the pyroprobe at any one time.

Off-line thermal desorption of silica trapped hypy oils The yields recovered from the off-line thermal desorption pyrolysis of the silica trapped hydropyrolysis oils are presented in Fig. 2. Although the total yield of products desorbed at all temperatures is significantly lower than that of the starting hydropyrolysis oil, the effect of temperature is apparent with a steady increase in the recovery of the aliphatic, aromatic and polar fractions from a final temperature of 300ºC through to 500ºC. The yield of aliphatic components at 500ºC is similar to that in the original hydropyrolysis oil, with the reduction in overall yield due to the poor recovery of the aromatic and polar fractions.

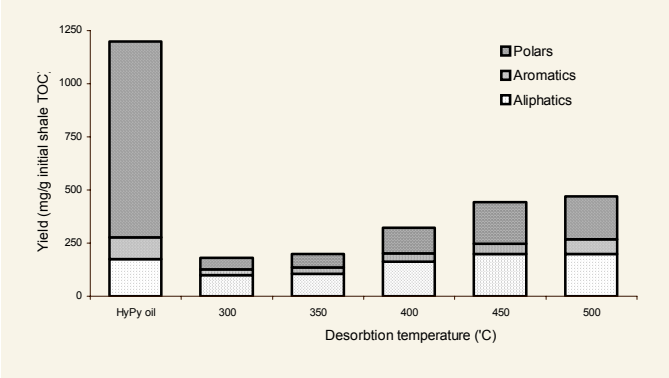

Figure 2. Yield (mg/g initial shale TOC) of aliphatic, aromatic and polar fractions in the thermally desorbed (off-line) Göynük oil shale hydropyrolysates compared to the original hydropyrolysate.

A significant proportion of the carbon in the hydropyrolysate was not desorbed from the trapping silica (131 mg/g initial shale TOC at 300ºC; 33 mg/g initial shale TOC at 500ºC). As noted for reduced yields of asphaltenes adsorbed on silica during hydropyrolysis, interactions between silica and polar functional groups in the sample my result in the reduced desorption of this fraction relative to the non-polar aliphatic and aromatic compounds.

The distribution of aliphatic hydrocarbons in the hydropyrolysate of GOS (Fig. 3A) is dominated a bimodal distribution of *n*-alkane /*n*-alk-1-ene doublets (maximum at C_{30} and submaximum at C_{21}), with the homologous series extending up to C_{40}.[(1)]. The *n*-alkanes are the more abundant, with an even-over-odd predominance (EOP) apparent among the longer chained homologues, and the distribution of *n*-alk-1-enes mirroring that of their saturated analogues. Such doublets are ubiquitous components of kerogen pyrolysates[(7)], although as noted earlier[(1)], the survival of *n*-alkanes heavier than ~C_{35} are not often observed in on-line pyrolysis experiments (e.g. Derenne *et al*.,[10]). Changes in the profiles with increasing desorption temperature can be assessed by measuring the ratio in abundance between a long chain alkane e.g. *n*-C_{30} and a relatively short chain one not subject to evaporative losses e.g. *n*-C_{18}.

This parameter may also vary as a result of cracking of the longer chained *n*-alkanes, which could potentially arise at higher desorption temperatures resulting in a concurrent increase in the abundance of the shorter chained homologues[11]. As indicated in Table 2, for desorption at 300ºC the higher molecular mass *n*-alkanes are clearly not desorbed efficiently as the doublet envelope has a different shape with a maximum abundance at C_{16}. However, desorption at 500ºC gives a profile is very similar to that of the original hydropyrolysate oil (Fig. 3B).

Table 5. Molecular abundance ratios to monitor secondary cracking during the thermal desorption of the silica trapped hypy oil. CPI after Philippi, 1965 = 2*C_{29}/(C_{28}+C_{30}).

Desorption T/ºC	*n*-C_{18} / *n*-C_{30} alkane	CPI[a]	Total alkanes / alk-1-enes
300	1.21	0.71	0.36
350	0.50	0.83	0.33
400	0.50	0.83	0.33
450	0.50	0.83	0.34
500	0.50	0.82	0.37
HyPy oil	0.33	0.79	0.30

Secondary cracking during both the hydropyrolysis and desorption phases would also result in a decrease in the magnitude of the EOP amongst the longer chained *n*-alkanes[3], which can be assessed by the carbon preference index (CPI), and lead to an increase in the abundance of the unsaturated *n*-alk-1-enes in these samples relative to the *n*-alkanes[12, 13]. These ratios for each desorption temperature are presented in Table 5, and suggest that with the exception of the poorly desorbed 300ºC sample, and some evidence of minor cracking at higher temperature, the distribution of these compounds in the desorbed oils are not that dissimilar to that of the original hydropyrolysis oil. Indeed, high recoveries of individual hopanes and steranes with no evidence of isomerisation and cracking were also achieved at 500ºC.

On-line thermal desorption of silica trapped hypy oils The on-line thermal desorption pyrolysis of the silica trapped GOS hydropyrolysate (Fig. 3C) resulted in greater evidence of secondary cracking than was apparent in the off-line studies. In addition to the generation of a higher proportion of shorter chain *n*-alkenes (*n*-C_{12} - *n*-C_{16}), the envelope of *n*-alkanes also shows a different pattern, with, in addition to the higher relative abundance of shorter chain *n*-alkenes, a maximum at *n*-C_{28} instead of *n*-C_{30} and fewer of the very long chain *n*-alkanes apparent. However, as with the off-line studies the recovery of high molecular mass extended hopanes and steranes with the biologically inherited and thermodynamically unstable stereochemistry, which would be the most susceptible to isomerisation and/or cracking of the alkyl side chain [3], suggests that the extent of cracking is not extensive. Thus, with scope for further optimization of the pyrolysis conditions, on-line thermal desorption shows considerably potential in retaining considerable more structural integrity than py-GC-MS for fingerprinting petroleum source rocks and coals.

Conclusions

It has been demonstrated that hypy oils can be recovered on silica and the quantitative recovery of hydrocarbons from a light crude oil desorbed from silica under hydropyrolysis conditions demonstrates no significant loss of the high molecular mass *n*-alkanes (>*n*C_{10}). The use of liquid nitrogen as the trap coolant results in significantly improved recovery of the lower molecular mass constituents. The silica-adsorbed oils undergo relatively little cracking during thermal desorption, with similar *n*-alkane and biomarker profiles being obtained as with normal work-up and GC-MS analysis. Thus, in terms of fingerprinting hydrocarbon moieties in geomacromolecules, hypy-GC-MS, in terms of retaining a high level of structural integrity is potentially an attractive alternative to traditional py-GC-MS.

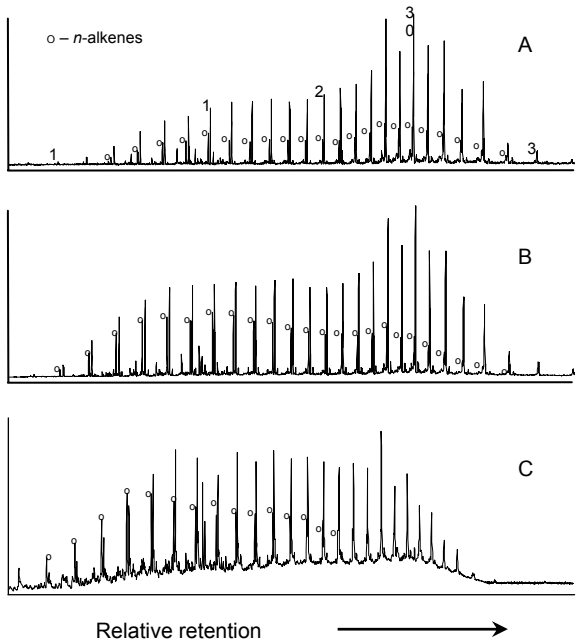

Figure 3. TIC of: A - the aliphatic hydrocarbon fraction of the GOS hydropyrolysate; B - the aliphatic hydrocarbon fraction of the oil recovered from the off-line thermal desorption at 500ºC of the silica trapped GOS hydropyrolysate; C - the on-line pyrolysis (700ºC) of the silica trapped GOS hydropyrolysate.

Acknowledgement. The authors thank the Natural Environment Research Council (NERC) for financial support (Ocean Margins LINK grants, nos. NER/T/S/2000/01366 and 2001/01153).

References

(1) Love, G.D., Snape, C.E., Carr, A.D., Houghton, R.C., 1995. *Organic Geochemistry,* **1995**, *23*, 981.
(2) Love, G.D., Snape, C.E., Carr, A.D., Houghton, R.C., *Energy & Fuels*, **1996**, *10*, 149.
(3) Love, G.D., McAulay, A., Snape, C.E., Bishop, A.N., *Energy & Fuels,* **1997**, *11*, 522.
(4) Bishop, A.N., Love, G.D., Snape, C.E., Farrimond, P., Organic Geochemistry, **1998**, *29*, 989.
(5) Murray, I.P., Love, G.D., Snape, C.E., Bailey, N.J.L., *Organic Geochemistry,* **1998**, *29*, 1487.
(6) Gallegos, E.J., 1975. Analytical Chemistry, **1975**, *47*, 1524.
(7) Larter, S.R., Horsfield, B., In Engel, M.H., Macko, S.A. (Eds.) *Organic Geochemistry*, **1993**, Plenum Press, New York. pp. 271.
(8) Philip, R.P., Gilbert, T.D., *Geochimica et Cosmochimica Acta*, **1985**, *49*, 1421.
(9) van Graas, G., *Organic Geochemistry*, **1986**, *10*, 1127.
(10) Derenne, S., Largeau, C., Casadevall. E., Tegelaar, E., de Leeuw, J.W., *Fuel Processing Technology*, **1988**, *20*, 93.
(11) Kissin, Y.V., *Geochimica et Cosmochimica Acta*, **1987**, *51*, 2445.
(12) Behar, F., Pelet, R., Roucache, J., *Organic Geochemistry*, **1984**, 6, 587.
(13) van Lieshout, M.P.M., Janssen, H-G., Cramers, C.A., van den Bos, G.A., J. of Chromatography A, **1997**, *764*, 73-84.

STUDY ON THE STRUCTURE OF ANTHRACITE BY ANALYZING ITS HYDROGEN CONTENT

Hiromi Aso, Koichi Matsuoka and Akira Tomita
(Institute of Multidisciplinary Research for Advanced Materials,
Tohoku University, Sendai 980-8577, Japan)
e-mail: tomita@tagen.tohoku.ac.jp

Introduction

There have been many attempts to elucidate the chemical structure of heavy hydrocarbons using various techniques [1-3]. The data of elemental analysis are the most important information among all [4]. However, the materials with more carbon and less hydrogen are quite difficult to analyze. In fact, little attention has been paid on the elemental analysis of carbonaceous materials. This is partly because the carbon content is overwhelmingly high and the contents of minor elements are too small to accurately analyze. The present paper attempts to make every effort to determine hydrogen content of carbonaceous materials as accurately as possible. After temperature-programmed oxidation (TPO) of hydrogen to water, careful analysis of water was made with gas chromatography and mass spectroscopy. It is definitely necessary to have reliable elemental analysis data for deeper understanding on the structure. For example, the accurate H/C atomic ratio can be used to directly speculate the size of aromatic ring system.

Experimental

Samples. In this study, three Chinese anthracites (<150 μm) were used as examples of carbonaceous materials. The ultimate analysis of the raw anthracites determined by a conventional method is presented in Table 1. These anthracites were demineralized by washing with HF and HCl solutions, and the effect of mineral matter removal on the hydrogen content was examined by comparing two sets of anthracites.

Table 1. Ultimate Analysis of Raw Anthracites

sample	code	ultimate analysis [wt %, daf[a]]			
		C	H	N	S+O[b]
Si Wang Zhang	SWZ	93.96	1.18	0.61	4.25
Men Tou Gou	MTG	95.69	1.16	0.25	2.90
Guo Er Zhuang	GEZ	96.27	1.32	0.66	1.75

[a]dry ash free [b]by difference

Apparatus. The reactor for TPO was a fixed bed reactor, which was made of quartz tube with an inner diameter of 7 mm. The gas analyses were made with a gas chromatograph and a quadrupole mass spectrometer. In order to remove H_2O in the carrier gas, a drying tube was installed before the reactor.

Procedure. About 200 mg of sample was fixed in the center of reactor using quartz wool. The reactor was purged with He gas flow until O_2, N_2, CO_2 and H_2O disappeared in GC signals. TPO was carried out by heating the sample under 5% O_2 in He (200 ml/min) at a rate of 2 °C/min up to 1000 °C and the temperature was kept at 1000 °C for 60 min. The gas products during TPO were continuously analyzed with GC and MS. Temperature programmed desorption, TPD, was carried out under a similar condition as TPO, except that pure He flow was used instead of O_2/He flow. We measured the amount of H_2O evolved during TPO and TPD mainly by GC. The GC response was calibrated using calcium oxalate monohydrate.

Results and Discussion

Gas Evolution during TPO and TPD. TPO patterns of raw anthracite are shown in Figure 1. H_2O evolution rate is shown in the upper panel, and CO/CO_2 evolution rate together with O_2 consumption rate are shown in the lower panel. Roughly speaking, two H_2O evolution peaks were observed for SWZ and MTG, and most of these peaks are composed of several sub-peaks. In the first H_2O-evolution range from 50 to 500 °C, no O_2 was consumed and no CO and CO_2 were formed. On the other hand, the H_2O evolution peak from 500 to 800 °C was accompanied by O_2 consumption and CO/CO_2 formation. It should be noted that GEZ gives no H_2O evolution peak at the low temperature region.

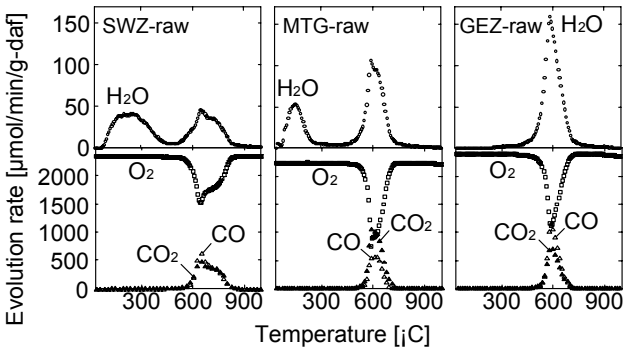

Figure 1. CO, CO_2 and H_2O evolution pattern and O_2 consumption pattern for raw anthracites during TPO.

The H_2O evolution pattern in the low temperature range between 50 – 500 °C was almost the same between TPO and TPD and also between raw and demineralized samples. In the higher temperatures, however, a very small amount of H_2O was evolved between 500 - 700 °C upon TPD of raw anthracite, and it disappeared if the demineralized sample was used.

H_2O Evolution in the Low Temperature Region. The lower temperature peak in Figure 1 can be due either to adsorbed water, dehydration of mineral matter or decomposition of hydroxyl group. Since the amount of H_2O evolved from raw anthracite in the low temperature region was almost the same as that for demineralized anthracite, dehydration of mineral matter would not be the main reason for the H_2O evolution in this region. Furthermore, the content of hydroxyl group in anthracite is very low [5]. The decomposition of surface functional groups, if any, can account only for a slight portion of H_2O evolution. Contrary to the above possibilities, H_2O desorption from anthracite would be more plausible explanation.

Careful examination on the H_2O adsorption and desorption behavior with these anthracites revealed that a considerable amount of H_2O was kept in MTG and SWZ anthracite even after He purge prior to TPO and TPD experiments. This adsorbed H_2O evolved in the region between 50 and 500 °C in both TPO and TPD. The adsorption rate as well as desorption rate with GEZ was much faster than the others. Thus, H_2O in GEZ was almost completely removed during He purge, and therefore no H_2O evolution was observed with GEZ in the low temperature region.

Small H_2O Evolution Peak at 500 - 600 °C. SWZ and MTG raw anthracites evolved a small amount of H_2O at around 600 and 530 °C, respectively, under TPD condition. It is likely that the origin of these small peaks were the dehydration of mineral matter, since these peaks were not seen in TPD of demineralized anthracites. Furthermore, the temperature range reported for the dehydration of

kaolinite is close to the small H_2O evolution observed at 500 - 700 °C.

H_2O Evolution in the High Temperature Region during TPO. Now we are in a position to discuss on the major part of H_2O evolution at high temperatures. These H_2O come from inherent hydrogen in anthracite, and thus the H_2O evolution should be closely related to the structure of anthracite. The H_2O formation pattern in the high temperature region during TPO is different in shape, temperature and quantity between three anthracites (Figure 1). This is undoubted indication of the different structure of these anthracites.

More detailed analysis of high temperature peak will be of great interest. A closer look at the H_2O evolution peak reveals that the peak in the high temperature region is composed of multiple peaks. This suggests that anthracite have several different types of hydrogen. The separation of these peaks was not attempted in the present study because of rather poor peak resolution. The quantification of well-resolved peak components will provide much more useful information on the structure of anthracite.

Implication of hydrogen content to the structure of anthracite. In TPO, hydrogen in anthracite was converted to H_2O, and carbon was converted to CO and CO_2. The atomic ratio of H/C in the evolved gas corresponds to the ratio of H/C in the anthracite molecule. To eliminate the contribution from mineral matter in the following discussion, the data on demineralized anthracites are used (Table 2).

Table 2. Gas Evolved from Dem-Anthracite in the High Temperature Range during TPO.

sample	gas	gas evolved [mmol/g-daf]	atomic ratio, H/C [-]
SWZ-dem	CO	28.0	0.08
	CO_2	47.8	
	H_2O	3.0	
MTG-dem	CO	33.9	0.13
	CO_2	44.1	
	H_2O	5.0	
GEZ-dem	CO	40.4	0.18
	CO_2	33.7	
	H_2O	6.8	

These values give straightforward information on the chemical structure of anthracites. The structure was speculated under the following assumptions: (1) anthracite molecule consists only of carbon and hydrogen, (2) the molecule has graphene-type hexagon, and (3) all peripheral carbon atoms are occupied with hydrogen. Under these assumptions, the H/C ratio of 0.08 for SWZ-dem corresponds to a hexagon of 469 rings and with an edge of 3.2 nm long, whereas that of 0.2 for GEZ-dem to a hexagon of 61 rings and with an edge of 1.2 nm long. Even though this is only average value and this was deduced from audacious assumptions, such calculation made it possible to visualize a remarkable difference between SWZ-dem and GEZ-dem. It is almost impossible to imagine this difference only from the elemental analysis data.

Another important message from this study is that the present result suggests the inadequacy of using ultimate analysis data to speculate the chemical structure of hydrocarbon sample. This becomes obvious if the H/C ratio from TPO result is compared with that calculated from the ultimate analysis (Table 1). The H/C ratio determined from the yield of H_2O, CO and CO_2 in the higher temperature region during TPO was 0.09, 0.14 and 0.20 for SWZ-raw, MTG-raw and GEZ-raw, whereas the H/C ratio calculated from ultimate analysis is 0.151, 0.145 and 0.165, respectively. The difference is incredible. The former value faithfully reflects the aromatic hydrocarbon structure of anthracite, but the latter does not. Hydrogen in ultimate analysis contains not only hydrogen in organic moiety but also hydrogen in adsorbed water and mineral matter.

Further comment should be made on the so-called coal rank. It is generally thought that the extent of coalification is higher for coals with higher carbon contents. In this sense, the rank among three anthracites should be SWZ < MYG < GEZ. However, the carbon content only in the organic portion of anthracite is 96, 97 and 98 wt % for GEZ, MTG and SWZ, respectively. From this viewpoint, the order of rank becomes GEZ < MTG < SWZ, which is opposite to the above order. Of course, the latter order is more meaningful. In this way, careful quantification of hydrogen content in carbonaceous materials provides various information of great value.

Conclusions

The hydrogen content in anthracite was carefully determined by TPO and TPD techniques. H_2O evolved from adsorbed water, dehydration of mineral matter, and decomposition of hydroxyl group was quantitatively evaluated, and the rest of H_2O evolution was attributed to that from organic portion in anthracite. This H_2O evolution constitutes the major portion of the TPO peak in the range of 500 - 800 °C. The yield of this H_2O together with those of CO and CO_2 gives an H/C atomic ratio of the anthracite molecule. Three anthracites used in this study gave the H/C ratio ranging from 0.08 to 0.18. The former value corresponds to a hexagon molecule with a size of 3.2 nm on average, while the latter corresponds to 1.2 nm. Ultimate analysis data cannot provide such essential information.

Acknowledgement. The anthracite samples used in this work were kindly supplied by Professor Peng Chen of Beijing Research Institute of Coal Chemistry.

(1) Hirsch, P. B. *Proc. Roy. Soc. A* **1954**, *226*, 143.
(2) Shinn, J. H. *Fuel* **1984**, *63*, 1187.
(3) Sharma, A.; Kyotani, T.; Tomita, A. *Energy Fuels* **2000**, *14*, 1219.
(4) Brown, J. K.; Ladner, W. R. *Fuel* **1960**, *39*, 87-96.
(5) Hatami, M.; Osawa, Y.; Sugimura, H. *J. Fuel Soc. Jpn* **1967**, 46, 819.